University of Bath

UNIVERSITY OF
BATH

PHD

Synchronously Pumped and Continuous Wave Mid-IR Hollow Core Fibre Gas Lasers

Abu Hassan, Muhammad Rosdi

Award date:
2017

Awarding institution:
University of Bath

Link to publication

Alternative formats

If you require this document in an alternative format, please contact:
openaccess@bath.ac.uk

Download date: 17. Aug. 2021

Synchronously Pumped and Continuous Wave Mid-IR Hollow Core Fibre Gas Lasers

Muhammad Rosdi Abu Hassan

A thesis submitted for the degree of Doctor of Philosophy

University of Bath
Department of Physics

September 2016

''Recite in the name of your Lord who created''-[96:1]

Abstract

The mid-infrared (mid-IR) spectral range between 3 and 8 µm is an area of growing interest for a range of applications, mainly in the fields of aerospace and sensing. This thesis describes the demonstration of a new form of the mid-infrared fibre laser, based on the use of acetylene in high-performance silica hollow core fibre. The first results of this work describe the fabrication and characterization of hollow core fibre that used in our laser system. The hollow-core fibre has the lowest-loss optical fibre in the 3 µm spectral band. The fibre attenuation of 0.025±0.005 dB/m was recorded. This enables us to demonstrate that this type of hollow core fibre can be used to make a novel form of a laser for the mid-infrared. Our laser consists of a hollow core fibre filled with an active gas – in our case, acetylene – and excited using a widely-available diode laser at 1.5 µm wavelength. We have demonstrated lasing on a number of transitions in the spectral band 3.1 – 3.2 µm. It lases either continuous wave or synchronously pumped when pumped by telecoms-wavelength diode lasers. The system is highly stable over long periods, in both CW and synchronously-pumped configurations. Studies of the generated mid-infrared output power, pump power threshold, and slope efficiency as functions of the input pump power and gas pressure have been performed and show an optimisation condition where the maximum laser output power is achieved for a given fibre length. This laser system could be extended to other selected molecular species to generate output in the spectral band up to 5 µm, and it has excellent potential for power scaling.

Acknowledgement

Table of Contents

List of figures

List of tables

CHAPTER 1

1.1 Lasers

For years, the laser has been a hallmark in science fictions yet much of our technology today depends on them. From DVD players, range finding devices, optical communication, and supermarket barcode scanners to laser pointers and Star Wars movies, lasers are part of our lives. The laser is a device that generates or amplifies light through a process of optical amplification based on the stimulated emission of electromagnetic radiation. The term "laser" stands for "Light Amplification by Stimulated Emission of Radiation" [1]. In 1960, Theodore Maiman demonstrated the first laser operation by shining a high-power flash lamp on a ruby rod with silver-coated surfaces [2].

The properties of laser light are fundamentally different from any thermal light source such as the flashlight. Lasers exhibit some unique characteristics. Firstly, laser light is highly monochromatic, which mean it has a single frequency, a pure colour and constant amplitude, in contrast with flashlight emits broadband continuum of light at many different wavelengths. Depending on the laser type, they can have wavelengths from the ultraviolet through the visible or in the infrared portion of the electromagnetic spectrum. The laser light also coherent; the wavelength has a consistent phase with time, which is called as temporal coherence. The laser emits light only in one direction compared to other conventional light source such as a flashlight, emits lights in all directions. The directionality of laser helps laser light to stay narrow over great distances

(collimation), enabling applications such as laser pointers. In laser light, energy is concentrated in small region space with greater intensity. Thus all these properties of laser light enable to use in the wide application.
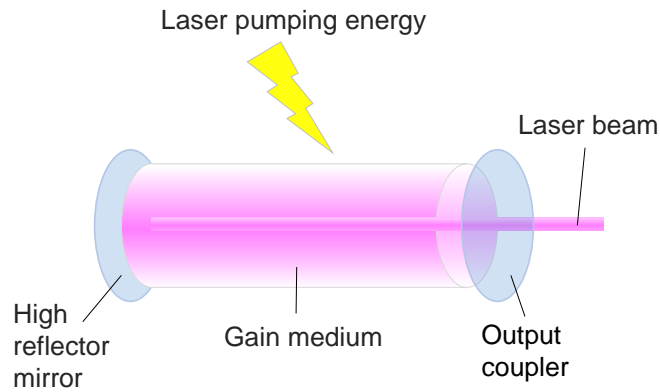
Figure 1 shows common laser construction.

The typical components of all lasers consist of a gain medium which can be gas, solid or liquid as illustrated in Figure 1. The gain medium is a material with properties that allows the amplification light through stimulated emission. Light of a single wavelength that passes through the gain medium is amplified (increase in terms of power/intensity). The input pump source of energy can be electrical such as high voltage discharge or optical like laser diode or flash lamp. The most common type of laser uses a resonator in the form of an optical cavity. The laser consists a high reflectivity mirror and partially reflecting mirror (output coupler) on each end of the gain medium. Light is reflected back and forth between the mirrors, passing through and being amplified by the gain medium each time. Some of the light escape through the output coupler. The light coming out of the laser may spread out or form a narrow beam.

1.1.1 How the laser works

The interpretation of light emission and absorption as proposed by Einstein [3] is an important tool for understanding the physics of the laser.
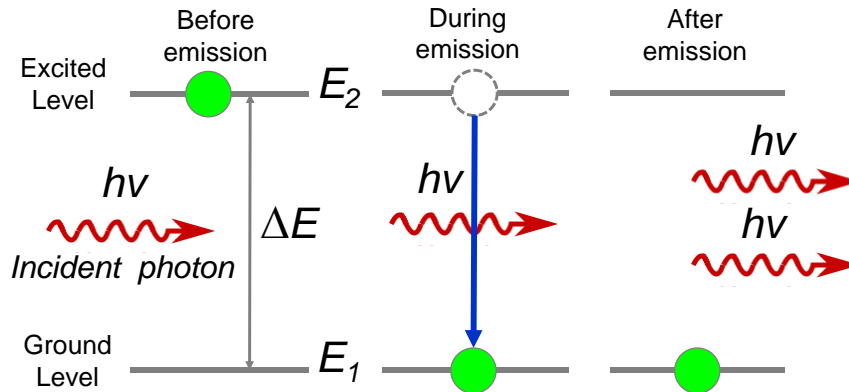
Figure 2 shows how the energy conversion happen.

In Figure 2, we indicate some ways in which energy conversion can occur. Let us consider two energy states of the electron. The ground state we denote as E_1 and excited state as E_2.

- When an electron absorbs energy from the incident photon, it receives that incident quantum of energy. Absorption of an increment of energy $\Delta E = E_2 - E_1$, from the pump. The atom is jumped from ground state to excited state.

- But the excited electron that jumped to higher energy state does not remain for a longer period in that state and it comes back to its original ground state by losing its energy in the form of photons. The photons do not have any correlation in phase and thus considered as incoherent light. Thus, the release of energy by electrons on their own, this is known as spontaneous emission. The transition of electrons from one state to another state occurs

3

randomly in time. Spontaneous emission is defined as the process in which the electrons in the excited atoms is released on their own from their higher energy state to the ground state.

- Now let us assume, coherent beam of light hν =E_2-E_1 incident from an external source on gain medium. The light energy in the form of photon stimulates electrons in the state N_2 to undergo a transition to the state N_1. The large of photons of the same energy is simultaneously emitted. Thus, the emitted photons have the property called as 'temporal coherence' and this process is called as 'Induced or stimulated emission'.

All these processes occur in the gain medium of the laser. The gain medium is pumped by an external source of energy (optically pumped, or an electrical field) into an excited state. In most lasers, this medium contains a population of atoms which have been excited into such a state using an external light source which supplies energy for atoms to absorb and be transformed into their excited states. The stimulated emission process is the basis for amplification in the gain medium. However, amplification can only take place when emission is greater than absorption. For that to happen, population inversion is needed. Let the number of electrons in E_2 state is said to be as N_2. The number of electrons N_2 in the state E_2 will be increasing rapidly by the supply of sufficient and appropriate energy to the active medium from an external source. At some point, a number of electrons N_2 in the state E_2 is greater than the number of electrons N_1 in the state E_1, i.e. N_2>N_1. This process is called population inversion. The process in which the number of electrons (N_2) in higher energy state of an active medium is increased to

a value greater than the number (N_1) in the ground state (i.e. $N_2 > N_1$) is called as Population Inversion.

When a gain medium is in enclosed state (cavity), multiple reflections of emitted light occur, where stimulated emission dominates spontaneous emission. Thus, the incident beam of light get amplified and results in output as a laser. The optical cavity typically comprises of two mirrors between which a coherent beam of light travels bi-direction, bouncing back on itself so that an average photon will pass through the gain medium repeatedly before it is emitted from the output coupler or lost to diffraction/absorption. If the amplification in the medium is greater than the resonator losses, then the power of the recirculating light can rise exponentially, and laser oscillation may initiate. The laser then saturates after the gain of its medium decreases. A steady state condition is reached when the net gain just equals the loss.

There are various types of lasers. The laser medium can be a solid, gas, liquid or semiconductor. The mediums can be selected based on the desired emission wavelength, the power needed, power efficiency and pulse duration. The list of the laser type with their common applications are shown in the table:

Table 1 Types of lasers and their applications.

Types	Applications
Solid-state lasers The active medium of a solid-state laser consists of glass or crystalline "host" material to which is added a "dopant" such as neodymium, chromium, erbium, or ytterbium.	YAG lasers emit infrared light at 1.064 µm used for drilling holes in metals. Pulsed lasers can be used in medical applications such as endoscopy.

Gas lasers A gas laser is a laser in which an electric current is discharged through a gas to produce coherent light.	CO_2 lasers emit energy in the far-infrared and are used for cutting hard materials. The helium–neon (HeNe) lasers are used in schools and laboratories because of their low cost and near perfect beam qualities.
Excimer lasers Use reactive gases, such as chlorine and fluorine, mixed with inert gases such as argon, krypton or xenon. When electrically stimulated, a pseudomolecule (dimer) is produced. When lasing, the dimer produces light in the ultraviolet range.	Widely used in high-resolution photolithography machines. Eye surgery (LASIK).
Dye lasers Lasers use complex organic dyes like rhodamine 6G in liquid solution or suspension as lasing media. They are tunable over a broad range of wavelengths.	Astronomy (as laser guide stars), atomic vapour laser isotope separation, manufacturing, medicine and spectroscopy.
Diode lasers These electronic devices are minuscule and use low power.	Telecommunication (pump diode), laser printers, barcode readers, image, laser medicine technologies.
Fibre lasers A fibre laser is a laser in which the active gain medium is an optical fibre doped with rare-earth elements such as erbium, ytterbium, neodymium, dysprosium, bismuth, praseodymium, thulium and holmium.	Material processing (marking, engraving, cutting), telecommunications, spectroscopy, and medicine.

1.1.2   Mid-IR laser

Since the first laser was invented, laser research has created a variety of improved and specialised laser types, optimised for different performance goals and applications. Mid-infrared (mid-IR) emission is currently an area of rapid development, with several competing technologies.

Many atmospheric species have a vibrational fingerprint in the 3-5 microns mid-IR region. Various molecules such as methane and carbon dioxide have a strong absorption wavelength in mid-IR range. There is a demand for a compact and stable mid-IR laser source to be used for highly sensitive environmental measurement and gas analysis.

Currently, the most commercially available and wide mid-IR laser in the market is a semiconductor laser [4]. The mid-IR semiconductor lasers are compact and electrically driven; namely, quantum cascade lasers (QCLs). Unlike typical interband semiconductor lasers that emit electromagnetic radiation through the recombination of electron–hole pairs across the material band gap, QCLs are unipolar and laser emission is achieved through the use of intersubband transitions in a repeated stack of semiconductor multiple quantum well heterostructures. These type of lasers use mature semiconductor materials like GaAs and InP to fabricate pn-junctions that incorporate energy well structures to produce a reduced band gap device effectively [5].

Quantum cascade lasers are consists of a periodic series of thin layers of semiconductor material, forming quantum energy wells that confine the electrons to particular energy states. As each electron traverses the lasing medium it transitions from one quantum well to the next, driven by the

voltage applied across the device. By suitable design of the layer thicknesses, it is possible to engineer a population inversion between two sub-bands in the system which is required in order to achieve laser emission. The electron continues through the structure and when it encounters the next period of the structure where another photon can be emitted. This process of a single electron causing the emission of multiple photons as it traverses through the QCL structure gives rise to the name cascade and makes a quantum efficiency of greater than unity possible which leads to higher output powers than semiconductor laser diodes.

Quantum cascade lasers are outstanding mid-infrared light generators with the ability to generate watt-level output powers [5]. QCLs have even been integrated with photonic crystal resonator structures [6]. QCLs do suffer from a few drawbacks. These types of laser emit a range of wavelengths covering from 3.5 microns. Moreover, QCL operation is facing a heat management problem. In the CW operation, more than 70% of injected electrical power is converted to heat from the 100 μm^2 regions of the active area [7]. Based on that, it will be some limitation to produce high power single mode from the QCL source. Additionally, the structures that determine the band gap are relatively complex, making fabrication of the devices relatively complicated and expensive.

The gas laser has long histories in generating mid-IR light [8],[9]. By using specific molecular gas that has a mid-IR transition (e.g., C_2H_2 and HCN_3), these lasers can be pumped using telecommunication bands where commercial pump sources (like erbium-doped fibre lasers and amplifiers) are well established and readily available to produce mid-IR emissions [10]. Gas laser offers some significant advantages compare to solid state

lasers such as high damage thresholds, good heat mitigation, and covers wide range emission wavelength from the near to far-infrared.

The main reason for using certain gas lasers preferable in the mid-IR region instead of solid-state lasers is that they offer wider transparency windows than their solid-state counterparts (QCL does not pick up until beyond 3.5 microns). In addition, gas lasers operate at many lines of vibrational-rotational molecular transitions have made it possible to cover some spectral intervals of the medium-IR range at a considerable level of both peak (10^6-10^8 W) and average (10-10^5 W) power [11].

The major drawbacks for the gas laser to integrate into the various practical optical application is the laser system is so bulky and fragile packaging required to realise long optical path lengths and extract appreciable laser output due to the dilute nature of gas media.

Fibre lasers have become ubiquitous over the last decade, mainly due to a few main features: high-efficiency conversion, compact packaging, high reliability, excellent beam quality, and broad gain bandwidth [12]. The highest values of solid fibre laser output power and efficiency have been achieved at around 1 μm by adding rare-earth elements like Yb^{3+} into the core [13].

Fibre lasers based on rare-earth-doped silica are very successful to around 2.2 μm wavelengths. To extend the emission wavelength from fibre lasers towards and into the mid-infrared will be necessary for a large number of existing and future applications. Unfortunately, the performance of silica fibre beyond the natural loss minimum of silicates at 1.5 μm remains a significant challenge. Beyond about 2.8 microns, conventional fibre lasers start to drop off [14]. Conventional optical fibres

formed from silica glass cannot be used in this spectral range because silica glass is strongly natural absorbing. The high phonon energy of silica glass means that it is not transparent beyond 2.4 μm and longer wavelength transitions are efficiently quenched by multi-phonon non-radiative decay. The fall in output power with increasing emission wavelength is caused primarily by the growing quantum defect between the pump photon energy and laser photon energy. The quantum defect is defined as the difference in pump photon energies and laser photon energies. The larger quantum defect at longer wavelengths creates heat that becomes an ever-increasing fraction of the absorbed pump energy.

At wavelengths beyond 3 μm, softer glasses like fluoride and chalcogenides are considered to have outstanding potential as hosts for rare earth elements. Currently, a high-power diode-cladding-pumped Ho^{3+} doped fluoride glass fibre laser operating in cascade mode have demonstrated mid-infrared emission at room temperature using diode pumping [15]. However, these glasses are hard to purify, are not always stable in ambient conditions, and difficult to draw into fibres.

We recognised that hollow core fibres could enable a new type of fibre laser. With the development of a new type of silica hollow-core fibres (negative curvature hollow core fibre) that performs extraordinarily well in the mid-IR region [16] provides an opportunity for efficient fibre gas lasers using hollow core fibres. The hollow core fibre gas laser combines attractive features of fibre lasers such as compactness, flexibility and the long interaction length of the pump and laser emission with those of gas lasers such as the potential for high output power and narrow linewidth.

The works are done here with the aim to explore further development in term of a novel form of a laser for the mid-infrared based on hollow core fibre. The laser consists of a hollow core fibre filled with an active gas – in our case, acetylene – and excited by using a widely-available diode laser at a shorter wavelength. The laser emits light at any of some wavelengths, selectable by tuning the pump laser. Because the laser is based on silica fibre, it should have some of the advantages of other fibre lasers which operate at shorter wavelengths, including the potential for high power operation. Being pumped with a diode laser makes it conceivable that this scaling to higher powers could be achieved cheaply and easily, using readily-available components.

1.2 Thesis Structure

We have structured the thesis as follow;

In Chapter 1 an overview of a laser is presented, highlighting the background of the development of the mid-IR laser as well the motivation behind the mid-IR laser development in this thesis. We have introduced the various type of laser that has been developed for the mid-IR region. Also, we have provided a brief comparison between different kinds of the lasers in term of the reliability, power performance, challenges that need to be addressed to emulate the successes of the lasers in telecom band. This chapter is necessary to ensure the reader understanding the motivation and the important of this works for the body of the knowledge.

Chapter 2 presents the background of a gas laser and the optical pumped molecular laser (OPML). The basic OPML scheme for mid-IR lasing also being studied. The acetylene molecular gas that is of interest to this thesis has been discussed in details. The spectroscopic data such as transition wavelengths and cross sections are provided for interpretations in the context of relevance to OPML applications. Last but not least, the analytical model using simple rate equations was presented can be used to estimate the initial performance of the laser system and help in further understanding the static and dynamic characteristics of lasers.

In Chapter 3, we describe a review covering the development of the negative curvature hollow core fibre in the mid-IR regions. The topics cover various types of NC-HCF core shape and their improvement made in term of attenuation of fibre. This chapter followed by a description of the guiding mechanism of the NC-HCF using ARROW mechanism. Then,

we presented the general fabrication steps and the fabrication process for negative curvature fibre. In the second part of the chapter, the design and properties of the hollow core that used in this research was investigated.

Chapter 4 describes experimental configurations and explained each component in the system. We also introduced the alignment technique that we used to obtain the ring cavity to enable the laser system works. The precision of cavity laser alignment helps to reduce the loss in the cavity laser system and allows the laser system operates in low pump threshold. We show our laser can operate in two modes; continuous and pulse operation. The development of the pump source for our laser will be discussed in here. The configuration of pump source for the pump to operate our laser system in pulse mode or continuous wave mode was presented.

The experimental work and analysis of CW mid-IR hollow core fibre gas laser are shown in Chapter 5. The configuration and characteristics of the CW operation mode are described. The spectra and pump power–laser output curves for different pump lines is presented. The results show, our laser has a remarkably low threshold of below 20mW and so can easily lase when pumped by an unamplified diode laser with standard telecoms grade stabilisation.

Chapter 6 describes experimental work and analysis of synchronously pumped mid-IR hollow core fibre gas laser. The configuration of the pulse operation are presented, follows by characterising the laser pump threshold of the system. The dependence of the laser output on the repetition rate are studied for the pulse operation system. In this chapters, a stable laser system was demonstrated in synchronously-pumped

configurations. In the reminders of this chapter, measurements of the RF spectra, optical spectra, and time dependence for at selected repetition rates are described.

Finally, Chapter 7 concludes the work done in this thesis and defines some future work for this research.

CHAPTER 2

2.1 Light and Gas Interaction

2.1.1 Introduction

Since first gas laser invented in 1960, many gas-based lasers have been built and used for many purposes [17]. Since that, the gas laser has been the subject of active research and development efforts resulting in rapid and significant advances in performance and device technology. A variety of optically pumped gas lasers have been demonstrated, from the earliest CH_3F [18], CO_2 [19], and OCS [20], to alkali vapour [21], CO [22] [23], HBr [24], C_2H_2 and HCN [25].

The common gas lasers include helium-neon, argon, or carbon dioxide. These gas lasers have a very high damage threshold and good heat mitigation technique that allow most of the gas laser to achieve extraordinarily high average output power. Diode-pumped alkali lasers (DPALs) have produced continuous wave (CW) and output powers as high as 145 W [26]. In optically pumped gas lasers, high quantum efficiency was achieved up to 98% in Rb laser [27] and slope efficiencies of 81% have been demonstrated [28].

Figure 3 shows the wavelength coverage of the doped solid fibre laser and the gas lasers depend on the active ions and active gas used. Solid-core fibre lasers typically operate in the 1 µm to 2 µm wavelength region.

The emission regions are determined by the active ions, for example, Yb, Er, Pr, Tm, with which the silica core is doped [29].

Gas lasers can cover additional emission regions depending on the active gas used as shown in Figure 3. For example, C_2H_2 and HCN molecule have emission around 3-5 µm. Laser operation further into the IR utilises rotation-vibration transitions in molecular gases, e.g., HBr/HI, CO, CO_2 [19],[23],[24]. Emission in the VIS and UV typically relies on electronic transitions, examples are HeNe lasers [30] and I_2 lasers [31].
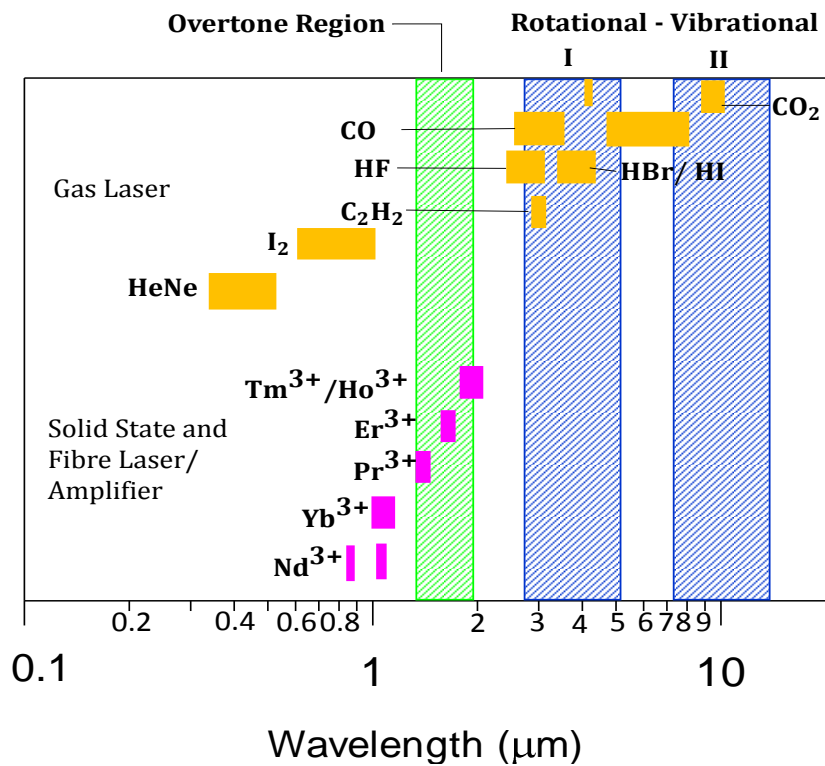
Figure 3 Examples of laser emission wavelengths from typical solid core fibre lasers with silica and possible emission wavelengths in gases. Shown are also the wavelengths of the two atmospheric windows I (2.9 – 5.3 microns) and II (7.6–16 microns), typically accessed for trace gas sensing. The data from [30].

The gas cell is usually used to contain gas in the gas laser system. In traditional gas cells, the effective interaction length is very short, and the laser system can be bulky and cumbersome, limiting their integration into many practical optical systems. The problem of weak interaction between light and gas can be solved with the introduction of gas-filled hollow core fibre. Hollow core fibre (HC-fibre) can function as unfolded cavities that permit long interaction lengths between the pump and generated laser light [32].

The HC-fibre offers many advantages to being use as a gain medium for a gas laser. One of the main benefits of using HC-fibre in developing a gas laser is that the interaction length could be extended, we can achieve very low thresholds and high efficiencies, and fibre-based systems have great potential for integration and reduction in size. Moreover, low-loss hollow-core fibre can be designed for restricted wavelength (for silica solid core fibre) regions such as 3-5 µm wavelength.

Compared with conventional solid fibre lasers, HC-fibre gas lasers can eliminate the nonlinear and damage limits which are due to the interaction between the light and solid material. The solid core silica fibre laser also suffer strong absorption near to mid-IR region which reduces its performance in the mid-IR region. Thermal effects may limit the output power that can be achieved in the solid fibre laser to protect from fibre end to damage. Based on this fact, the HC-fibre gas laser, is the alternative candidate compare to solid core fibre as a gain medium for the laser to operate in the mid-IR regions.

2.1.2 Optically Pumped Molecular Laser (OPML)

Optical pumping is a process in which light is used to pump electrons from a lower energy state in an atom or molecule to a higher energy state. It is commonly used in laser, to pump the active laser medium so as to achieve population inversion. Molecular vibrational-rotational transitions have narrow band transitions. The availability of the various high power coherent pump sources allows these narrow band transitions to be excited efficiently. The optical pumping is widely used due to the high selectivity of excitation is required, and also adaptability of the technique to a variety of different molecules makes it particularly suitable for a search of new infrared laser emissions. The molecular gases lasers operating in mid-infrared are based primarily on vibrational-rotational transitions.

The mid-infrared optically pumped molecular laser (OPMLs) can be categorised into several schemes. There are three possible combinations for the pump and the lasing transitions both of these can be strong (fundamental band transitions) or one strong and the other weak (overtone, combination or difference band transition). The first scheme is shown in (Figure 4 (a)), the same vibrational band (but different vibration-rotation transitions) are used both for pumping and lasing. In the second scheme (Figure 4(b)), the fundamental vibrational band is excited, and lasing happens on the difference band which corresponds to a transition from one vibrational mode to another. Here, by contrast, pumping is realised at the strong transition and lasing happens at the weak one. Third scheme (Figure 4(c)) is called the hot band, the combination or overtone transition. The hot band is a transition between two excited vibrational states. Whereas combination bands transition, which is involved

simultaneous excitation of multiple normal modes with a single photon and overtones, which are transitions that involve changing the vibrational quantum number for a normal mode by more than 1. In this scheme, a comparatively weak combination band is pumped, and a strong one is used for lasing.
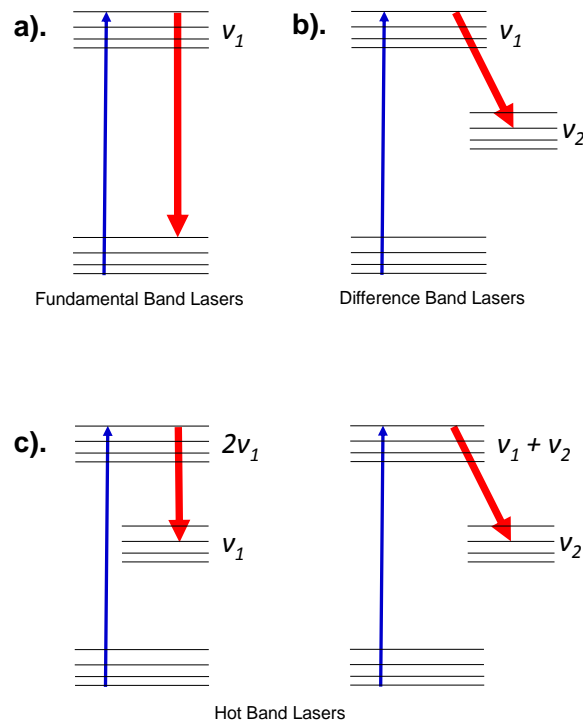
Figure 4 Energy level schemes for mid-infrared optically pumped molecular gas lasers. In fundamental band lasers, both pump and the lasing transitions are in the same fundamental band. In other band lasers, a fundamental band transition is pumped and emission is on a difference band. In hot band lasers, a combination level or an overtone level is excited and lasing is on a hot band transition.
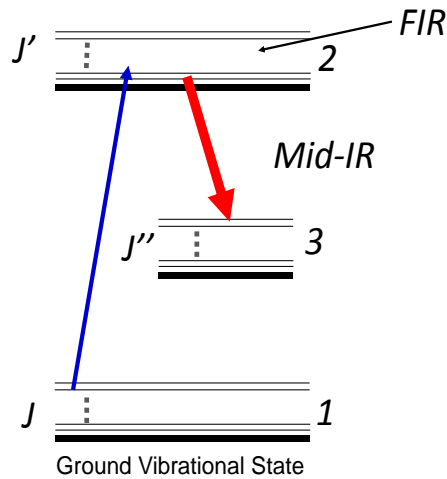
Figure 5 Simplified energy level diagram.

The basic operating principle of OPMLs can be understood by referring to the simple energy level diagram of a molecule used to our model shown in Figure 5. State 1 represents the vibrational ground state. State 2 accounts for the excited state. State 3 represents the laser terminal state. The basic operating principle of OPMLs can be understood by referring to the representative partial energy level diagram of a molecule shown in Figure 5. The molecules are pumped and excited from the vibrational ground state via rotational-vibrational transitions in the excited state and lase on transitions from this pumped state to rotational-vibrational states. Each vibrational energy states 1 to 3 comprise a significant number of rotational states. Under the action of resonant or near-resonant optical excitation of a vibrational-rotational transition, coherent emission can occur either on a purely rotational transition leading to far-IR (FIR) emission or on a vibrational-rotational transition resulting in mid-IR emission.

The excited state population that does not contribute to stimulated emission (lasing) can transfer energy to other rotational levels or

vibrational levels mediated by collisions. Thus, the laser gain will depend not only on the strength of the pump and lasing transitions but also on competing for relaxation processes. Therefore, the performance of OPMLs is controlled by the interplay between the pump transition, the laser transition and the collision induced population transfer processes.

Under resonant optical pumping using a laser or thermal radiation, field-induced transitions take place which may result in a none-equilibrium distribution of molecules over the vibrational and rotational levels and give rise to a population inversion and amplification at certain transitions. In studying the kinetics of the inversion under the action of resonant radiation, one has to take into account the following: apart from stimulated transitions; collisional processes of the molecular relaxation in the gas occurs; resulting in strong coupling between the resonant levels and those which do not interact directly with the radiation. Such collisional processes bring back the molecules to equilibrium in the end. It is the relaxation processes that determine the basic requirements placed on the parameters of a pump source: its intensity, pulse duration and frequency of radiation.

The knowledge of molecular physics is needed to understand how the optically pumped molecular lasers (OPMLs) works. Unlike solid state active medium, the gain spectrum of molecular gases is comprised of narrow transitions that represent the rotation-vibration energy level structure of molecules. Next, we will look into the potential candidate gas media for our laser system. This new class of 'hybrid' fibre-gas lasers holds the potential to generate diffraction limited beams in wavelength regions and at power levels beyond the fundamental limitations of rare-earth doped solid core fibre lasers.

2.2 Molecule candidate as active gain media

Table 2 lists few examples of active gas media with pump and lasing parameters. Among of them, C_2H_2 and HCN are an attractive, active gas prospect. Both C_2H_2 and HCN have strong absorption in the 1.52-1.55 µm region [33],[34] and hence are well suited for optical pumping in the fibre optic communication C-band, for example, with erbium fibre lasers. C_2H_2 and HCN have been shown to lase in the 3.1 microns (our interest wavelength) when optically pumped at 1.5 µm in conventional gas cells [25]. In this respect, C_2H_2 and HCN are the potential active gas candidates for our experiment. However, in the present works we have restricted ourselves to C_2H_2 molecule as a gain media.

Table 2: List of active gas media with pump and lasing parameters [35]

Gas	Pump			Lasing		
	λ (µm)	Vibrational State	Cross-section (cm^2)	Vibrational Transition	Cross-section (cm^2)	λ (µm)
C_2H_2	1.52	$v_1 + v_3$	8.8×10^{-18}	$v_1 + v_3 \rightarrow v_1$	2.8×10^{-16}	3.1
HCN	1.53	$2v_3$	4.1×10^{-18}	$2v_3 \rightarrow v_3$	4×10^{-16}	3.1
HCN-CO	1.53	$2v_3$	4.1×10^{-18}	$v = 3 \rightarrow 1$	1.1×10^{-17}	2.36
HI	1.54	$v = 3$	2×10^{-19}	$v = 3 \rightarrow 2$	9.7×10^{-18}	4.76
CO	1.57	$v = 3$	1.5×10^{-20}	$v = 3 \rightarrow 1$	1.1×10^{-17}	2.36

Since 1975, the researcher has explored the used of C_2H_2 for active gain media in lasing either using discharge pumping [36] or optical pumping [37]. The first 3 µm radiation emission in the hollow core fibre filled with acetylene gas was reported in 2010 by Dr K.Corwin group at Kansas. The laser produces mid-IR emission (3.1-3.2 µm) by optically pumping with

1.52 µm, nanosecond pulses and based on population inversion [38] with few percent due mainly to linear losses of the fibre at the laser wavelengths. In 2011, they estimated the slope efficiency of fibre gas laser system limit up to 27% by improved the attenuation of the hollow core fibre [39] while the desired slope efficiency was not achieved.

Recently, Wang *et al.* demonstrated high repetition rate and a reduction of saturation effects in a diode laser pumped acetylene filled negative curvature hollow core fibre laser. A system using acetylene as a gain medium can be pumped using a stabilised, modulated, fibre amplified diode laser around 1530 nm [10]. In those experiments, although amplification of spontaneous emissions was enhanced by the waveguiding provided by the fibre, there was no cavity feedback/resonator and only pulsed single-pass operation was reported. Pump peak powers of tens of watts were required for appreciable conversion [25],[39] while the continuous wave (CW) operation was not achieved.

2.2.1 C_2H_2 molecule as active gain media

C_2H_2 molecular has five normal modes of vibration. C_2H_2 molecules are linear and symmetric. The normal modes of vibration for the C_2H_2 molecular are shown in Figure 6. The notation of C_2H_2 (v_1 v_2 v_3 v_4 v_5) stands for the energy levels of the vibrational normal modes.
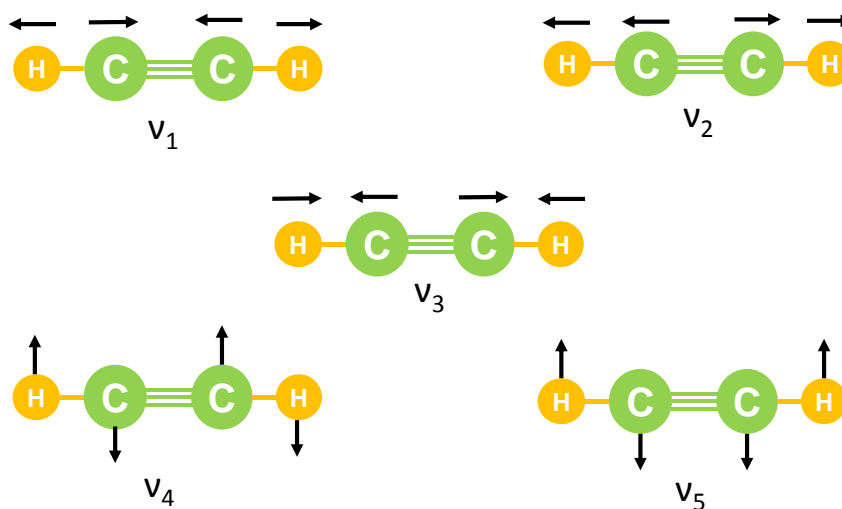
Figure 6 The vibration normal modes of C_2H_2.

Acetylene has five vibration normal modes which are three stretching modes and two bending modes. The v_1 and v_3 modes correspond to the symmetric and antisymmetric C – H stretch; the v_2 mode corresponds to the C – C symmetric stretch; and the v_4 and v_5 modes correspond to the symmetric and antisymmetric C – H bends. The two stretching modes are doubly degenerate as two orthogonal bending modes could be created simply by rotating the molecule 90° about the internuclear axis [40]. The pump transition at 1.5 µm corresponds to the (00000) → (10100) transition.

24

Figure 7 (a) shows the simplified energy level diagrams and associated with each vibrational level labelled (v_1 v_2 v_3 v_4 v_5) for C_2H_2 is a rotational ladder. The spacing of rotational energy levels to first order is independent of the vibrational state and is given by $2B(j + 1)$, where B is the rotational constant of the vibrational state and j is the rotational quantum number. At room temperature, according to the Boltzmann distribution, maximum population occurs in the rotational state with $j = 9$ for C_2H_2. As the R-branch transitions correspond to $\Delta J = +1$, they always occur at higher energies than the P-branch transitions, and thus always absorb or emit light at shorter wavelengths than P-branch transitions. This can be seen directly from the v_1 + v_3 rotational-vibrational overtone absorption spectrum of acetylene shown in Figure 7 (b). No Q-branch transitions are observed since there is no angular momentum associated with either the v_1 or v_3 vibrational modes.
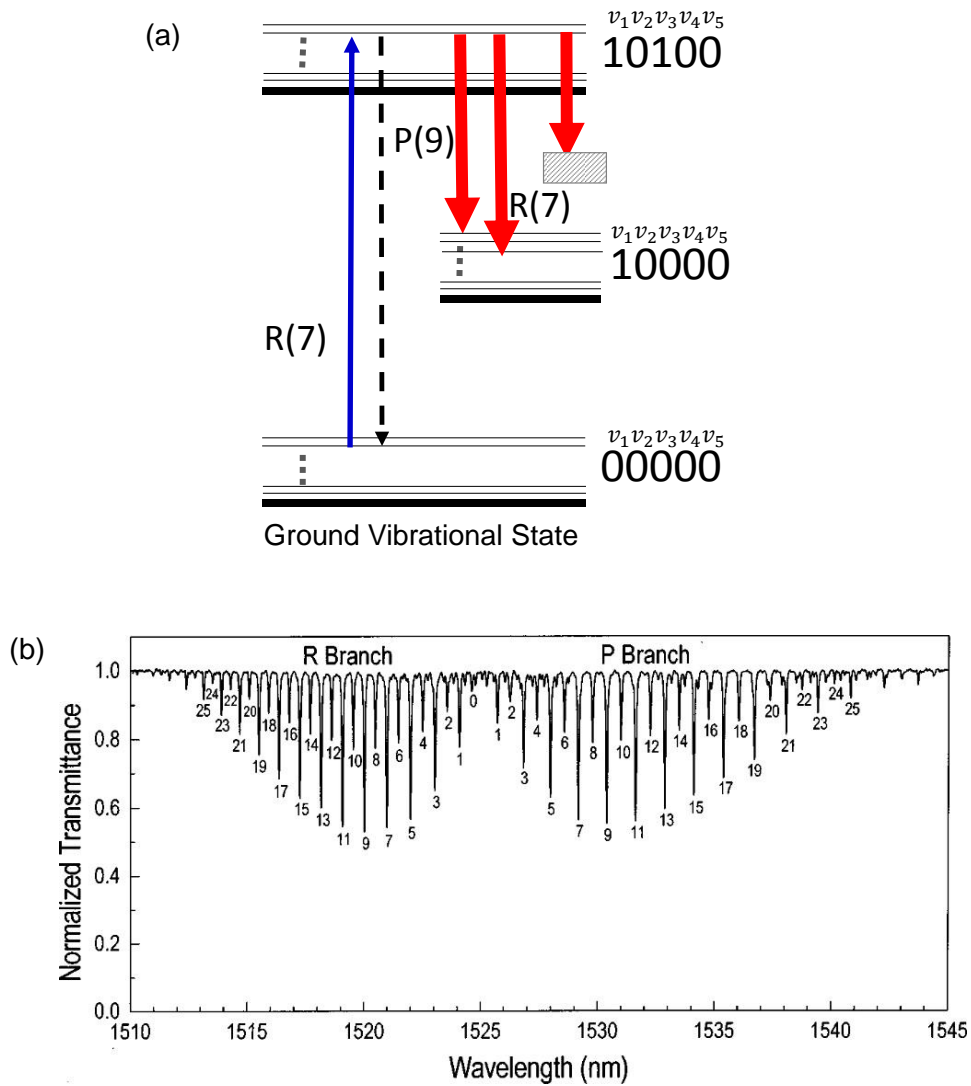
Figure 7 (a) Energy level diagram of acetylene molecule. The blue arrow denotes the pump transition at 1.5 μm. The dashed arrow indicates the non-radiative transition back to ground state. The red arrows indicate the lasing transitions at 1.5 μm and 3 μm respectively as examples. The grey box stands for other potential lasing transitions of acetylene. (b) Absorption spectrum of $^{12}C_2H_2$ molecules contained in a 5-cm long gas cell showing the R and P-branch transitions between the vibrational ground state and the $v_1 + v_3$ vibrational state. Taken from Reference [41].

Table 3 Example on possible of dipole-allowed transitions of acetylene originating from the terminal pumped state (10100).

Dipole allowed transition	Approximate wavelength of transition(μm)
(10100)→(00000)	1.5
(10100)→(00010)	1.6
(10100)→(01000)	2.1
(10100)→(00100)	3
(10100)→(10010)	3.7
(10100)→(11000)	7
(10100)→(11010)	14

There are several potential lasing transitions as listed in Table 3. From the [42], the absorption cross-section for (00000)→(10100) is ~ 8.8×10^{-18} cm^2. The lifetime due the spontaneous emission of (10100) → (00000) is about 0.1 s. The emission cross-section for (10100) → (10000) is estimated to be about 2.8×10^{-16} cm^2. The lifetime due to the spontaneous emission (10100) → (10000) is about 0.017 s. It should be mentioned that vibrational relaxation of C_2H_2 due to collisions with buffer gases has been reported for the (00100) state [43]. However, the energy pathway of the collision has not been identified. The collision time between molecules of the order of 10^{-7} s.

2.2.2 Analysis of rate equations

The analytical model using simple rate equations can be used to predict laser output, optimum pressure and incident pump threshold from the acetylene filled hollow core fibre. The energy level system for acetylene molecule is complex. In acetylene case, the transition from laser states to the vibrational ground state is dipole forbidden. The acetylene molecule in laser state only can depopulate to ground level by the collision. To start

27

with, we assume simple 4 level system, where the laser transition ends on a level above the ground state. A simplified schematic vibrational level system of the acetylene molecules is shown in

Figure **8**. The state 0 represents the vibrational ground state. State 3 represents the excited state. States 2 and 1 represent the terminal laser states. In acetylene case, the transition from laser states to the vibrational ground state is dipole forbidden. The acetylene molecule in laser state only can depopulate to ground level by the collision.
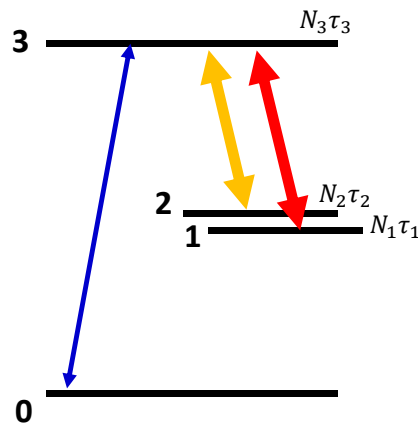
Figure 8 Simplified energy level diagram for acetylene. Four-level energy level diagram used to model gas-filled hollow-core fibre laser. State 0 is the ground state. State 3 is the pumped excited state. States 2 and 1 represent the two terminal laser states, which not couple directly to the ground state.

The rate of change in the number of molecules in the state N_i (molecules/s) in steady state can be written as:

$$\frac{dN_1}{dt} = \frac{\sigma_l I_l}{h v_l} (N_3\text{-}N_1) - \frac{N_1}{\tau_1} = 0 \tag{1}$$

$$\frac{dN_2}{dt} = \frac{\sigma_l I_l}{h V v_l} (N_3\text{-}N_2) - \frac{N_2}{\tau_2} = 0 \tag{2}$$

$$\frac{dN_3}{dt} = R_p - \frac{\sigma_l I_l}{h v_l} (N_3\text{-}N_1) - \frac{\sigma_l I_l}{h v_l} (N_3\text{-}N_2) - \frac{N_3}{\tau_3} = 0 \tag{3}$$

$$\frac{dn_{l1}}{dt} = \frac{\sigma_l I_l}{h v_l} (N_3\text{-}N_1) - \frac{n_{l1}}{\tau_{o1}} = 0 \tag{4}$$

$$\frac{dn_{l2}}{dt} = \frac{\sigma_l I_l}{h v_l} (N_3\text{-}N_2) - \frac{n_{l2}}{\tau_{02}} = 0 \tag{5}$$

$$N_3 = N_2 + N_1 \tag{6}$$

Where n_{l1} and n_{l2} are the photon densities of the laser light; σ_l and σ_p is laser emission cross section and absorption cross section respectively (m^2); I_l and I_p is laser and pump intensity (watt/m^2); τ is relaxation time (s) and the pump rate (molecules/s), $R_p = \sigma_p I_p \Big/ h V_p$ (N_t), with h is Planck's constant (m^2 kg/s), V_p is pump frequency (s^{-1}) and N_t is total molecule density (molecules/m^3).

Solving equations (1), (2), (4) and (5) in steady state where $I_l = chv_l n_l$, where c is speed of light (ms⁻¹), h is Planck's constant (m² kg/s), and n_l is laser photon density (molecules/m³).and V_l is laser frequency (s⁻¹) become:

$$(N_3 - N_1) = \frac{1}{\sigma_l \, c \tau_{o1}} \qquad (7)$$

$$(N_3 - N_2) = \frac{1}{\sigma_l \, c \tau_{o2}} \qquad (8)$$

$$\frac{N_1}{\tau_1} = \frac{n_{l1}}{\tau_{o1}} \qquad (9)$$

$$\frac{N_2}{\tau_2} = \frac{n_{l2}}{\tau_{o2}} \qquad (10)$$

Re-arrange equation (6) to $N_3 = (N_3 - N_1) + N_1$ and assume $\tau_o = \tau_{o1} = \tau_{o2}$, we can add equation (7) and (9) into equation (6) became:

$$N_3 = \frac{1}{\sigma_l \, c \tau_o} + \frac{n_{l2} \tau_2}{\tau_o} \qquad (11)$$

The cavity lifetime, $\tau_o = (L + L_g)/c/(-\ln(1 - L_f) - \ln(R_m))$. Where τ_o, the photon cavity lifetime (s), L is the cavity length (m) and L_g is the length of the gain medium (m). The cavity life time determine by the reflectance, R_m of the output coupler and combined other linear loss per round trip L_f.

Re-arrange equation (3), assume $\tau = \tau_1 = \tau_2 = \tau_3$ and add term (7), (8) and (11) into equation (12) becomes:

$$R_p = \frac{\sigma_l\, I_l}{hv_l}(N_3 - N_1) + \frac{\sigma_l\, I_l}{hv_l}(N_3 - N_2) + \frac{N_3}{\tau_3} \tag{12}$$
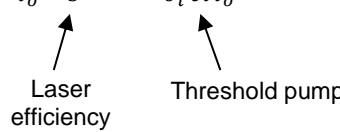
$$R_p = \frac{\sigma_l\, chv_l n_l}{hv_l}\left(\frac{1}{\sigma_l\, c\tau_o}\right) + \frac{\sigma_l\, chv_l n_l}{hv_l}\left(\frac{1}{\sigma_l\, c\tau_o}\right) + \left(\frac{1}{\sigma_l\, c\tau\tau_o} + \frac{n_l}{\tau_o}\right) \tag{13}$$

$$R_p = \frac{n_l}{\tau_o} + \frac{n_l}{\tau_o} + \frac{1}{\sigma_l\, c\tau\tau_o} + \frac{n_l}{\tau_o} \tag{14}$$

$$R_p = 3\frac{n_l}{\tau_o} + \frac{1}{\sigma_l\, c\tau\tau_o} \tag{15}$$

Equation (15) can be re-arranged in term of total intracavity photon densities per round trip and becomes:

$$\frac{n_l}{\tau_o} = \frac{1}{3}\left(R_p - \frac{1}{\sigma_l\, c\tau\tau_o}\right) \tag{16}$$

Laser efficiency

Threshold pump

From Eq. (16), the pump photon rate must be larger than $1/(\sigma c\tau\tau_o)$ to lase. The threshold pump photon rate (molecules/s) can written as:

$$R_{th} = \frac{1}{\sigma_l\, c\tau\tau_o} \tag{17}$$

From our rate equation analysis, the predict laser efficiency is 33%. With all assumption made, the analytical prediction of laser efficiency seems to be reasonable due to the fact the maximum quantum efficiency of this kind

of transition is 50%. In chapter 5, by using a numerical model, we will compare the performance with the real experimental results to validate the assumption that we made in the analytical model.

2.3 Conclusion

Chapter 2 presents the background of the gas laser and the optical pumped molecular laser (OPML). The basic OPML scheme for mid-IR lasing also being studied. The acetylene molecular gas that is of interest to this thesis has been discussed in details. The spectroscopic data such as transition wavelengths and cross-sections are provided for interpretations in the context of relevance to OPML applications. Last, but not least, the analytical model using simple rate equations was presented can be used to estimate the initial performance of the laser system and help in further understanding the static and dynamic characteristics of lasers.

CHAPTER 3

3.1 High-Performance Negative Curvature Hollow Core Fibre for Mid-IR Regions

The "hollow core optical waveguides" referred to long cylindrical tubes and rectangular stripes made of dielectric or even metal. The potential of hollow core fibre made of a metal material for long haul electromagnetic wave transmission theoretically has been proposed by Carson *et. al* in 1936 [44]. Later, the feasibility of using the dielectric HCF in telecommunications has been studied by Marcatili and Schmeltzer [45]. They demonstrated analytically that the trade-off between modal leaky loss and bending loss would fundamentally limit the application of dielectric hollow core fibre for long-haul optical signal transmission.

In the late 20th century, the development of hollow-core photonic bandgap fibre (HC-PBG) speeded up the development of HCFs in both theory and applications immensely [46],[47]. Besides the new concepts of light guidance in HCFs and boosted the emergence of fibre optics. Moreover, inspired more novel designs of microstructure fibres in order to enhance the performances of the fibre. The state-of-the-art HC-PBGs already demonstrate extremely low transmission loss, comparable to that of commercial optical fibres [48]. They also have a very high damage threshold [49] very low group-velocity dispersion and an optical nonlinearity that is many orders of magnitude less than that of competing fibres [50].

Kagome fibre also was a part of HCF family. "Kagome" fibre was firstly reported in 2002 [51]. The Kagome fibre usually exhibits multiple transmission bands and overall covers a broader spectral range than HC-PBGs. Numerical simulations show that the "Kagome" lattice supports no photonic bandgap which makes the Kagome fibre distinctive [47], [52].

Another type of HC fibre was the negative curvature hollow core fibre (NC-HCF). With the simple cladding design and negative curvature core wall, NC-HCF combine the strength and durability of silica with record low attenuation in the 3–4 μm spectral band, where their attenuation can be 10,000 times less than that of bulk silica [16], [53], [54], [55], [56].

As in previous chapters, we mention the advantages of hollow core fibre gas laser compare to solid core fibre laser for the mid-IR region. In this chapter, we describe a high performance of the negative curvature hollow core fibre (NC-HCF) used in the mid-IR gas laser covering the review development, guiding mechanism and fabrication technique. Then, follow by the characterisation of the performance of NC-HCF.

3.2 Development of Negative Curvature Hollow Core Fibres

Negative curvature hollow-core fibre (NC-HCF) is a novel type of hollow core fibre, which is characterised by the negative curvature of core wall shape [57]. Such fibre exhibits multiple spectral transmission bands and can guide light in the hollow core with low attenuation over lengths of hundreds of metres. The exceptional qualities of NC-HCF's, such as low transmission loss, extended transmission wavelength and low latency and nonlinearity lend these fibres to a wide range of applications. The low-loss transmission windows in NC-HCF can span from visible to mid-infrared wavelengths [57] and have been successfully applied in transmission of high power lasers [58], the design of mode-locked fibre lasers [59] and study of nonlinear optics in gas [60]. Moreover, the simple structure of fibre cladding, allow tuning flexibility of NC-HCF's design and dimension of to meet the specific wavelength and application requirement [61],[62],[63],[64].

In 2010, Kagome hollow-core fibre with negative curvature core boundary results lower attenuation than conventional kagome fibre [65]. Results from that, a series of subsequent experiments have been done and confirmed the importance of core wall shape in the reduction of attenuation in such fibres [66]. In 2011, a group led by Pryamikov attempt to fabricate the simple structure of hollow core which is used only eight capillaries as a cladding. This fibre is the first NC-HCF made and operated in 3 μm wavelength [67].

In 2013, Fei Yu reported transmission in 3.1-microns region with minimum attenuation of 34 dB/km. He called 'core ice-cream shape of cladding' that

have curvature towards the core that affects the attenuation of the fibre. Later, the fibre was successfully applied for invasive surgical laser procedure in delivering high energy microsecond pulses at 2.94 μm [49]. Later, Kolyadin *et al.* purposed more simple design of the cladding structure of the NC-HCF to improve the attenuation in the mid-IR region. He reported the open boundary of core wall in NC-HCF, which is the contactless capillaries in the cladding. He demonstrated low loss transmission of light in the mid-infrared spectrum range from 2.5 to 7.9 μm [62]. Then, Belardi *et al.* demonstrated significantly reduced the bending loss of the similar shape of fibres in 2014 [68].

NC-HCF can be designed to guide light in an empty or gas-filled hollow core. Since as much as 99% of the optical power in these fibres can travel in air and not in the glass, they do not suffer from the same limitations to loss as conventional fibres and can exhibit radically reduced optical non-linearity, making them promising candidates for future ultra-low loss transmission fibres. Since that, NC-HCF has applied in many applications. Setti *et al.* were realised terahertz guidance in polymethyl-methacrylate in 2013 [69]. Besides that, NC-HCF also has implemented in high power laser [70],[71] delivery and have been applied in the study of gas-light interaction.

Here in this chapter, we will present works done to fabricate low-loss NC-HCF in this wavelength range. We start with describing the guiding mechanism of the NC-HCF using Antiresonant Reflecting Optical Waveguide (ARROW) mechanism. Then, we will explain the fibre draw technique and the NC-HCF technique fabrication process. The characteristics of the NC-HCF will be described later.

3.2.1 The importance negative curvature

NC-HCFs are characterised by the negative curvature of the core wall, which has been numerically and experimentally demonstrated to effectively reduce the attenuation. Numerical studies showed that in NC-HCF an increase of negative curvature influences the mode attenuation and even bending loss in a complex way [84]. It has been confirmed that a large curvature of the core wall (small radius of curvature) can help decrease the overlap of core mode field with fibre materials to 10^{-4}. This has been experimentally and numerically demonstrated in silica NC-HCFs [85], [84]. Despite recent efforts in the analytical analysis [86], the function of the core wall shape is not yet clear. It appears that both the properties of the high-index and of the low-index cladding modes are affected by the curvature.

3.3 Guiding mechanism
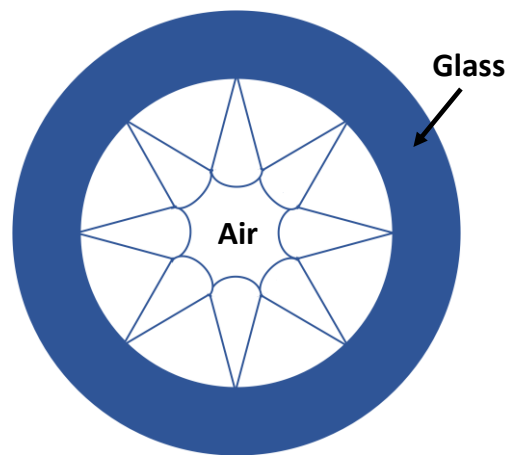
Figure 9 Schematic representation of the cladding of a negative curvature hollow core fibre. The core is surrounding by the negative curvature cladding that guided the light in the core.

NC-HCF has a simple structure as shown in Figure 9. It has no periodic cladding and does not possess a photonic bandgap, which explains the leaky nature of such fibre. The leaky nature and antiresonant guiding mechanism make it natural to compare NC-HCF with Kagome fibre. Both have multiple transmission bands and similar attenuation figures at comparable wavelengths [72],[73].

3.3.1 Antiresonant Reflecting Optical Waveguide (ARROW)

The guiding mechanism of NC-HCF can be simply explained using Antiresonant Reflecting Optical Waveguide (ARROW) model. The ARROW model was firstly proposed in 1986 to explain the enhanced confinement in a planar waveguide with a series of high-low index regions forming the cladding [74] [75] [76]. In 2002, it was used to provide a simple way to understand the light transmission in hollow core photonic bandgap HC-PBG fibre regarding waveguide theory more rather than the tight binding theory [77]. Soon it was being applied to a range of micro-structured HCF's.

The ARROW model is based on a consideration of the individual modes of the high index regions. It approximates the cladding of HC-PBG as an array of high and low refractive index layers. Each higher refractive index layer can be considered as a Fabry–Perot resonator as shown in Figure 10 [34].
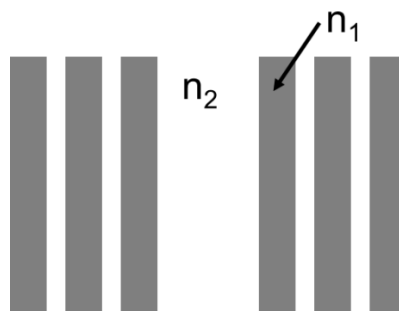
Figure 10 Schematic diagrams of a one-dimensional anti-resonant planar waveguide (the core is running vertically). In this cases high index regions, n_1, are darker grey and the low index background material, n_2, is white.

39

For one-dimensional case, when the wavelength of light in the core matches a resonant wavelength of the Fabry-Perot, the light will leak out of the core and confined in the high-index region, n_1 but if they are in anti-resonance wavelength with high-index region, n_1 the light will be confined back to the low-index core, n_2 of the waveguide as shown in Figure 10.

In the resonance in the 2-D waveguide, when the wavelength of light in the core matches a resonant wavelength of the Fabry-Perot cavity, the light will leak out of the core through the high index layer, n_1. As the wavelength is far away from the resonance of the cladding, the light will be reflected back and more strongly confined in the core, n_2 of the waveguide. NC-HCF possesses multiple transmission bands, and the band edges are determined by the resonance wavelengths of cladding as described by the ARROW model.
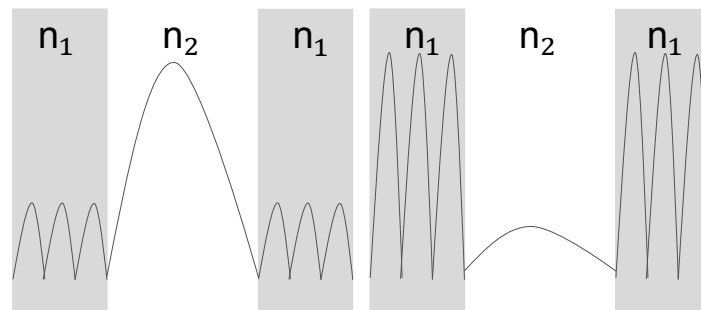
Figure 11 Schematic representations of the intensity profile in the core region and first high index regions in the one-dimensional planar waveguide. In both cases high index regions, n_1, are darker grey and the low index background material n_2 is white, a) is the anti-resonant case where light is confined to the core region by anti-resonant reflections and b) is when the wavelength is close to a resonance of the high index regions corresponding to the peak transmission of the Fabry-Perot cavity

The ARROW model explained the waveguide characteristics based on ray optics principle. ARROW cannot predict the loss magnitude or any other band details either. There is others model can be used to explain the guidance mechanism of NC-HCFs and other leaky HCFs, which is Marcatili and Schmeltzer model [45], and the coupled mode model [78]. Although the ARROW model is far from perfection, it is still widely acknowledged as one of the most effective and frequently used models to understand leaky HCFs.

3.3.2 Marcatili and Schmeltzer's Model

In 1964, Marcatili and Schmeltzer firstly analytically studied the mode properties of the dielectric HCF [45]. In their pioneering work, they derived formulas of mode attenuation and bending loss, which revealed the basic properties of modes in HCFs. A HCF consists of a circular core surrounding by the infinite homogenous non-absorptive dielectric medium of higher refractive index than the core material (usually gas/vacuum). Due to the inverted refractive index contrast, total internal reflection cannot occur when the light is incident from the core at the interface between the core and cladding. The partial reflectivity at the core boundary indicates an inevitable loss for light propagating in the core. The mode attenuation and corresponding propagation constant are written as [45];

$$A_{vm} = \left(\frac{u_{vm}}{2\pi}\right)^2 \frac{\lambda^2}{r^3} \, \mathrm{Re}(V_v) \tag{18}$$

$$\beta_{vm} = \frac{2\pi}{\lambda} \left\{ n_{core} - \frac{1}{2} \left(\frac{u_{vm}}{2\pi}\right)^2 \left[1 + \mathrm{Im}\left(\frac{(V_v \, \lambda)}{\pi r}\right)\right] \right\} \tag{19}$$

Here u_{vm} is the m_{th} zero of the Bessel function J_{v-1}, and v and m are azimuthal and radial number of modes; λ is the wavelength; r is the core radius; n_{core} is the refractive index of core medium; V_v is the constant determined by the cladding refractive index and mode order [45]. Equations (18) and (19) are the most basic formulas to understand modes in all leaky HCFs. As r/λ grows bigger, the attenuation of modes is quickly reduced. For a mode of a specific order, a higher propagation constant is required to satisfy the transverse resonance condition in a bigger core. Such larger core would give an increased glancing angle of light incident at the core boundary, which results in a higher Fresnel reflection. As a result, the mode in a larger core has a smaller attenuation. Marcatili and Schmeltzer's model fails when complex structures are introduced to the cladding of HCF. The multiple reflections from the structured cladding can reduce or increase the attenuation of leaky modes by constructive/destructive interference, and it affects the dispersion of modes too.

3.3.3 Coupled-Mode Model

The coupled-mode model applies coupled mode theory [78] to analyse the properties of HCFs based on Marcatili and Schmeltzer's model. In real HCFs, the cladding is no longer an infinite and homogeneous medium but

has a complex configuration of refractive index distribution. The cladding modes are a set of modes including both dielectric modes localised in the higher index regions and leaky air modes inside lower index regions [79], [80]. In the coupled-mode model, the properties of core mode are interpreted as results of the longitudinal coupling with those cladding modes. This method was successfully applied in analysing the formation of bandgaps in HC-PBG [81]. By this method, inhibited coupling was proposed to explain the guidance in Kagome fibre [52]. In 2007, Argyros and his colleagues applied the coupled mode theory to the square lattice polymer HCF and quantitatively analysed the formation of band edges of leaky HCF [82]. They pointed out that the absolute phase matching is not necessary to achieve an effective coupling between the cladding and core modes. $\Delta\beta \sim 10^{-4}$ m was found to be the threshold to estimate the transmission band edge, which matched well with the experimental measurement [82]. In 2012 Vincetti and Setti applied this method to NC-HCF and presented details of cladding mode features in NC-HCF [80]. Later, they used this method to demonstrate that the geometry of cladding elements was important to determine the confinement loss of HCFs. The polygonal shaped tube in the cladding adds extra loss due to the Fano-like coupling between the core and cladding modes [83]. This can be used to explain the different spectral features between NC-HCFs and Kagome fibres.

3.4 Fabrication of Negative Curvature Hollow Core Fibre

Negative Curvature Hollow Core Fibre (NC-HCF) is unlike conventional fibre is typically fabricated from only one material, the most commonly pure silica. The fabrication procedure for negative curvature hollow core fibre differs completely from that used for conventional step index fibre as the microstructure usually comprises glass and air. The simple one layer cladding of NC-HCF make it easy to stack but need attention to details when it draws to fibre. As the guiding mechanism differs between the conventional optical fibres, the fabrication process also differs as the cladding requires a proper structural arrangement to obtain high-performance NC-HCFs.

Here in Bath, we are mainly using the stack-and-draw technique to fabricate our NC-HCF structures. This method is inherited from photonics crystals fibre (PCF) fabrication technique [87]. There are other techniques to form the preform such as extrusion [88], [89], [90] and sol-gel casting [91], [92] that not be discussed in this thesis.

3.5 Stack and Draw

The fibres are fabricated using an adapted stack and draw procedure starting from commercially available synthetic fused silica tubing. The main reason to use the stack and draw technique is because it offers high flexibility in designing the fibre structure, low cost, speed and repeatability. Moreover, this flexibility allows us to design a negative curvature fibre. Figure 12 shows scanning electron microscope (SEM) images of few

types of NC-HCFs with different cladding structures with special fibre properties.
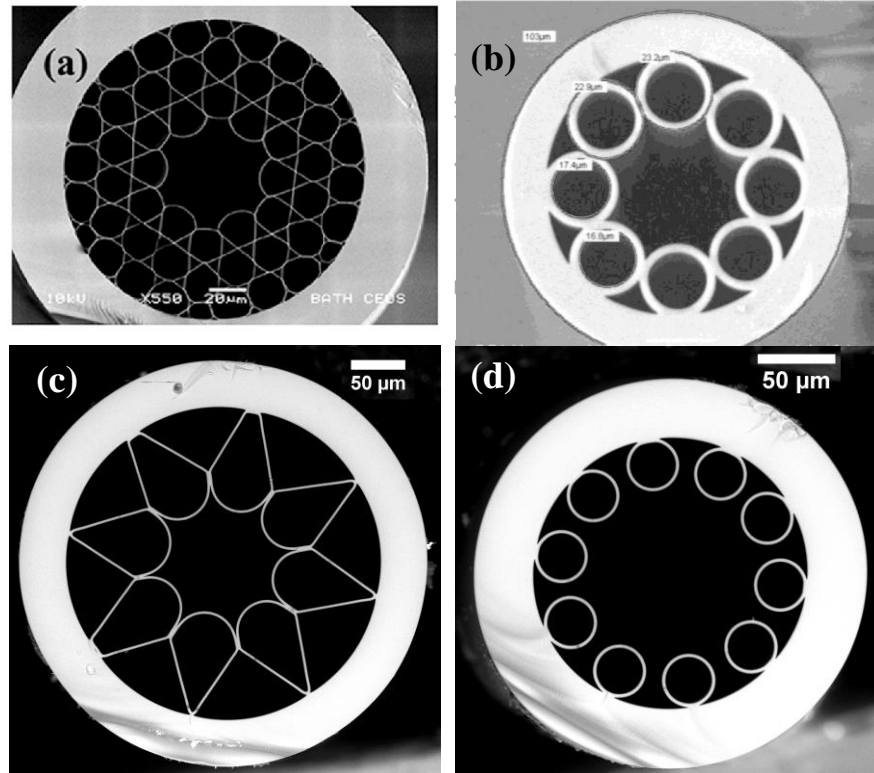
Figure 12 Scanning electron microscope pictures of few types of negative curvature fibre; a) hypocycloid-core Kagome hollow-core photonic crystal fibre [65]**, b) is negative curvature fibre from Pryamikov group** [67]**, c) Ice cream shape NC-HCF from** [16]**, d) NC-HCF made of silica, with non-touching capillaries fabricate by Belardi et. al.** [63]**.**

The stack and draw technique and fibre drawing of NC-HCF that used in this work are shown in Figure 13. In the stack and draw technique, the general step is to stack silica capillary tubes or solid silica rods into the desired pattern to produce a preform. The precision and uniformity while stacking capillaries and rods are essential because these will affect the properties and quality of fibre structure after the preform is drawn to fibre.

45
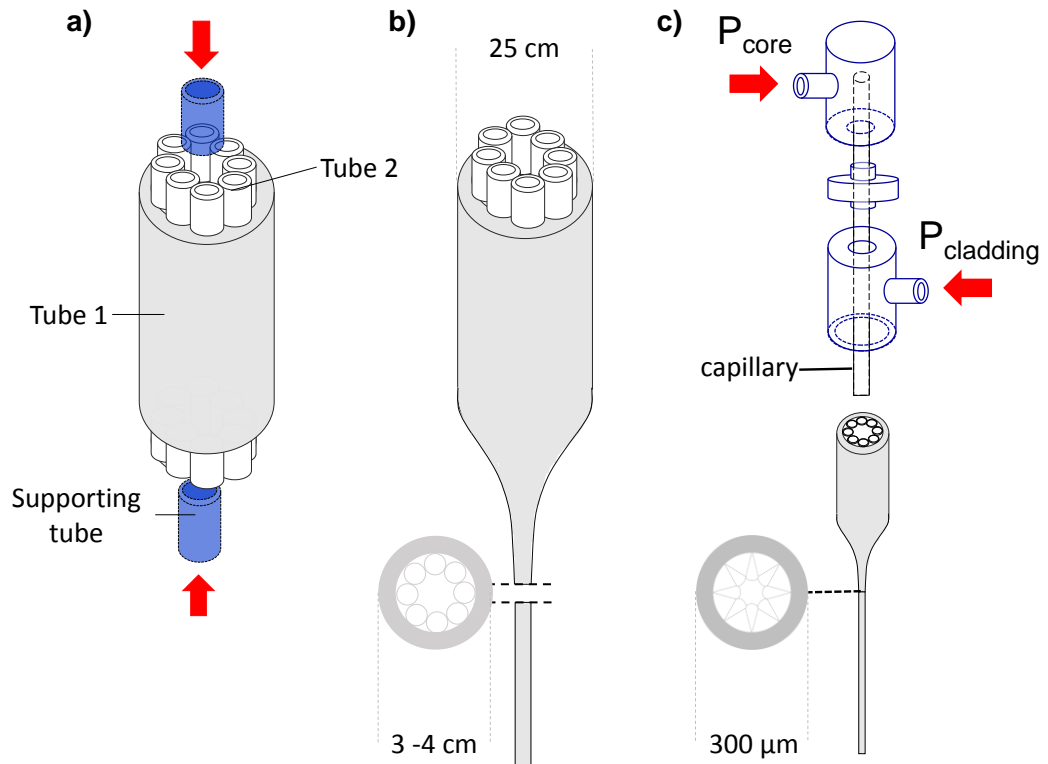
Figure 13 Three stages of the stack and draw technique of NC-HCF. (a) The first stage is stack the desire cane. To maintain the cladding structure, two short capillaries (blue tube) are to insert to both ends as support. (b) Drawing of canes. The middle part of stack without supporting capillaries is drawn into canes of smaller diameter. (Typically cane diameter is 3-4 cm). (c) Fibre fabrication from canes. Different pressures are applied to different regions of core and cladding.

All material used in fabrications presented in this thesis was F300 synthesised fused silica material from Heraeus which has a low concentration of OH- group [93]. We started with two tubes different outer and inner diameter was used tube 1 has an outer diameter (OD) 16.03 mm and 12.27 mm of inner diameter. Tube 2 has an outer diameter (OD) 25.1 mm and 23.39 mm of inner diameter. Tube 1 will be a jacket tube, and tube two will draw to a smaller diameter to stack inside the tube 2.

3.5.1 Stack

The fibre was fabricated using the stack and draw technique, by placing eight identical capillaries drawn from thin wall silica tube (Suprasil F300, Heraeus) inside a larger jacketing tube. To fabricate NC-HCF, two short capillaries (blue) or rods need to be inserted in the core region at the ends of the stack to support the cladding and prevent the stack from collapsing and to make sure the stack tight and does not slip out during the drawing process as shown in the Figure 13(a).

3.5.2 Drawing of cane

The cane is an intermediate preform which is drawn from the stack (Figure 13 (b)). The cane is essentially a complete optical waveguide but on the millimetre scale. The drawing of the cane is a necessary and important step in the fabrication of NC-HCF and other HCFs. One of the reason is to avoid a drastic scale change from the stack of the preform (centimetre scale) to final end-product (fibre) in micrometre scale. In the reference [94] mention, to preventing the structure from deformation becomes more problematic in the large scale change. Conclusions, drawing fibre from the smaller cane more rather than a bigger stack is a best practice to obtain a high quality of NC-HCFs. In our fabrication of NC-HCF, the cane size was usually about 3 – 4 cm in diameter.

3.5.3 Drawing of fibre

Next process, the cane is drawn to the fibre size using the fibre drawing tower as shown in Figure 13 (c). In this process, the end of the cane is installed to the brass metal holder. This particular design holder has a small hole to apply pressure into the cane to maintain air holes from collapse in the drawing process. The pure nitrogen usually used for pressurisation. The pressurisation is crucial not only to avoid the air holes from collapse during the drawing process, but also the key to the formation of the negative curvature core wall. The negative curvature core wall can affect the attenuation and the mode profile of the hollow core fibre.

While the fibre been drawn, the feed speed of the cane, the draw speed of the fibre, the furnace temperature and the gas pressure must be carefully adjusted, or the fine structure of fibre can be easily deformed otherwise. In the drawing stage, polymer material will be coated around the final fibre for protection and enhancement of the mechanical strength of the optical fibre. The parameter to obtain the NC-HCF are used in this thesis are presented in Table 4.

Table 4 Fibre drawing parameters to obtain NC-HCF for 3.16 µm wavelength.

Feed rate (mm/min)	Draw speed (m/min)	Tempreture (^oC)	P core (kPa)	P cladding (kPa)
50	6.6	1910	0.1	6

3.6 Design & Properties of Fibre

3.6.1   Fibre Design

The silica-based hollow fibres used in our experiments offer a complementary approach to fibre lasers in the mid-IR and are shown in Figure 14. Our works used two different hollow core fibres with slightly different designs. First, is the hollow core with un-touching capillaries in the cladding and second is the 'ice cream shape' in the cladding. This fibre will be our gain fibre and feedback fibre respectively. The similarity features of both fibres are negative curvature core boundary wall. The negative curvature core boundary provides a lower attenuation in interested wavelength for both fibres [54].
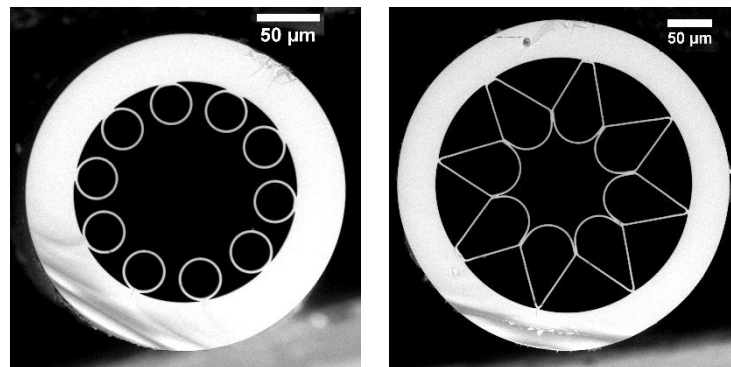
Figure 14 Scanning electron micrographs of the two different forms of hollow fibre used in the laser system. Left: gain fibre with transmission at 1.53 and 3.1 μm wavelengths. Right: feedback fibre with low loss at 3.1 μm.

First, the anti-resonant hollow core fibre used as a gain fibre was fabricated by one of our group members and reported in [68]. This fibre was choose because it has low attenuation at the pump band around 1.53 µm and also low attenuation at the lasing wavelength around 3.1 µm as shown in Figure 15. The gain fibre has a core diameter of ~109 µm, an outer diameter of ~233 µm, an average "cladding capillaries" diameter of 27.9 µm, and a silica wall thickness of ~2.4 µm.
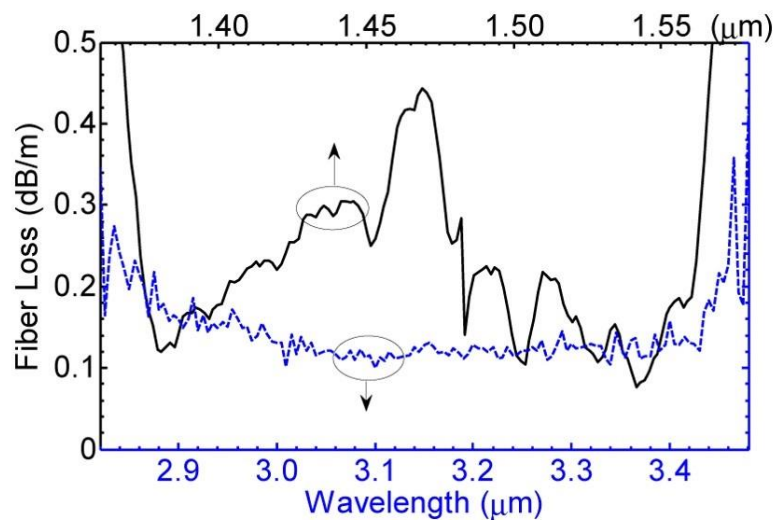
Figure 15 The measured transmission loss of the anti-resonant HC-PCF at shorter (solid line, top x-axis) and longer (blue dash line, bottom x-axis) wavelength. This figure is from [10]**.**

Secondly, the ice-cream shape is called a negative curvature fibre (NCF) was specially design to provide the lowest possible attenuation at the lasing wavelength. The NCF was used as a feedback fibre. It has a core diameter of ~95 µm, an outer diameter of ~357 µm, as shown in Figure 14 (b). We will discuss more technique used to obtain NCF attenuation in the next section.

3.6.2 Attenuation measurement: Cutback method

Attenuation is among of the main characteristics of the fibre. Attenuation of an optical fibre is the loss of optical power as a result of leakage, scattering, bending, and other loss mechanisms as the light travel through the fibre. The cutback method is often used for measuring the total attenuation of an optical fibre. The cutback method involves comparing the optical power transmitted through a longer piece of fibre to the power transmitted through a shorter piece of the fibre.

The cutback method involves comparing the optical power transmitted through a longer piece of fibre to the power transmitted through a shorter piece of the fibre. The cutback method requires that a test fibre of known length (L) be cut back to a shorter length (L_c). The cutback method begins by measuring the output power, P_y of the test fibre of known length (L). Without disturbing the input conditions, the test fibre is cut back to a shorter length (L_c). The output power, P_x of the short test fibre (L_c) is then measured, and the fibre attenuation is calculated. The attenuation of the cut piece can be determined by:

$$\alpha(\text{dB/m}) = \frac{10log_{10}(P_x/P_y)}{L-L_c} \qquad (20)$$

The standard cutback technique is a destructive technique which means the fibre under test to determining certain optical fibre transmission characteristics, such as attenuation and bandwidth. To avoid cutting the feedback fibre, we have measured the fibre attenuation accurately by using a modified version of the conventional cut-back technique in which

we use low loss butt-coupling (see Figure 16), which is repeatable, instead of cutting the fibre, which is not. Butt-coupling has a very low loss (< 0.1 dB) in these fibres because of the low numerical aperture, large core size and absence of Fresnel reflections. The uncertainty in the loss measurement is ± 5 dB/km. The fibre was loosely coiled on the bench with a bend radius of 40 cm to avoid additional loss caused by bending.
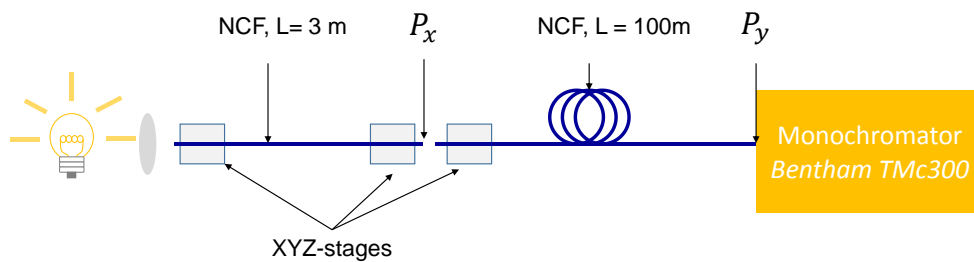
Figure 16 Schematic of the modified version of the conventional cut-back technique using to determine attenuation for feedback fibre.

In this section, all the cut-back measurements were performed by using a tungsten lamp which exhibits a broad spectrum from near-UV to mid-IR. In our experiments, all the spectra were measured and recorded by the optical spectrum analyser (OSA) *Ando AQ 6315A* (wavelength range from 350 nm to 1750 nm) and a scanning monochromator *Bentham TMc300* (wavelength range from 250 nm to 5.4 μm).
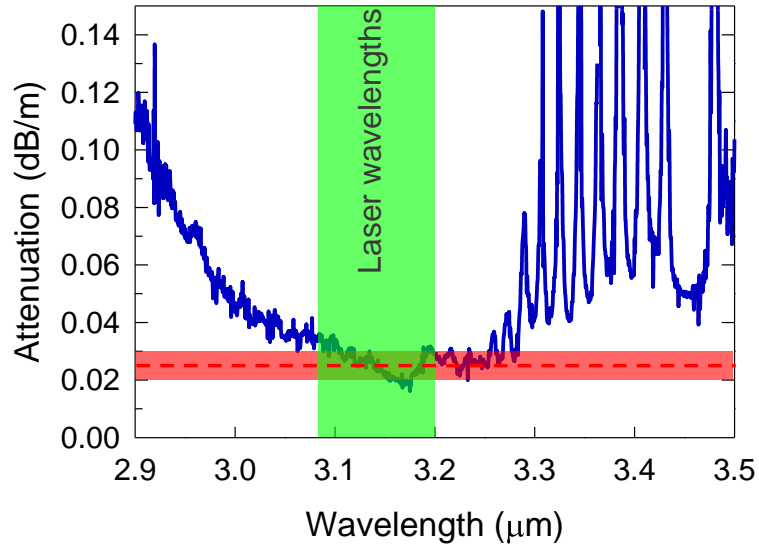
Figure 17 Attenuation curve for the feedback fibre, showing an attenuation of 0.025 ±0.005 dB∕m over the laser wavelength band. Sharp features at 3.3 μm and beyond arise from small quantities of HCl gas present in the fibre core. The pink band indicates the uncertainty in the measurement of minimum attenuation.

Figure 17 shows attenuation curve for the feedback fibre, showing an attenuation of 0.025 ±0.005 dB∕m over the laser wavelength band. Sharp features at 3.3 μm and beyond arise from small quantities of HCl gas present in the fibre core. The presence of trace amounts of HCl gas in our fibre would appear to be reasonable given that our starting material is F300 synthetic fused silica, which the manufacturer's state contains 1450 ppm of chlorine [95], and our measurement is over 100 m in length. We can remove those absorption lines by purging the fibre with nitrogen.

The red band indicates the uncertainty in the measurement of attenuation. Later, we will remeasure the attenuation using single wavelength laser to validate the accuracy of our measurement. Our feedback fibre (ice-cream cone shape) has one of the lowest attenuations reported for any optical fibre in this spectral band [96].
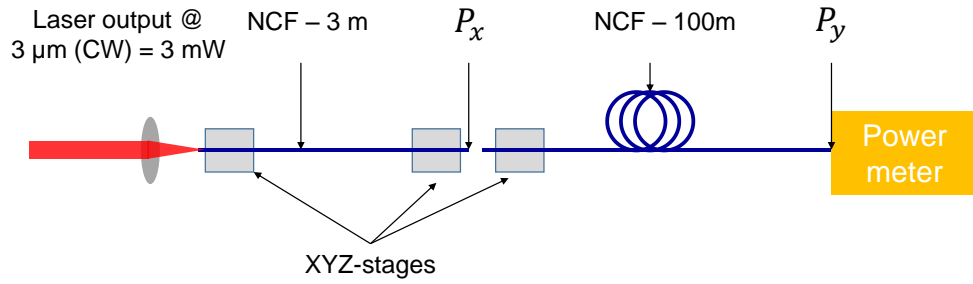
Figure 18 Schematic of the modified version of the conventional cut-back technique using to determine attenuation for feedback fibre.

The disadvantage of the tungsten lamp is its limited luminance especially at wavelengths above 3 µm in the mid-infrared spectral region. To validate our attenuation measurement for feedback fibre using tungsten lamp, we used our own CW 3 µm laser (as describe in Chapter 5) as a source to remeasure the fibre attenuation. The cut-back measurements were performed by replacing tungsten lamp with our stable CW 3 µm laser and the output measured using a power metre as shown in Figure 18. Measurements of optical powers were performed using a thermal power metre (*Ophir 3A-SH*). Table 5 lists the readings of the attenuation at 3.12 µm using stable CW laser. We measured three readings with the average attenuation 0.0298 dB/m, slightly higher compared to the attenuation using tungsten lamp due to a smaller fibre coiled radius causing the bending loss increased. However, the attenuation is still in the acceptable range and shows agreement with the last measurement.

Table 5 Readings of the attenuation of the NC-HCF using single wavelength laser.

P_x (mW)	P_y (mW)	Loss (dB/m)
0.600	0.303	0.0297
0.605	0.309	0.0292
0.615	0.304	0.0306

3.7 Conclusion

Chapter 3 presents the study of design and properties of negative curvature fibre. The step by step fabrication method of NC-HCF using stack and draw was shown. The cut-back measurement is the main method to determine the attenuation of NC-HCF experimentally. Although it is simple in measurement, many factors can influence the accuracy of measurement results.

We presented the attenuation curve for both gain fibre and feedback fibre. The gain fibre has a low attenuation at the pump band around 1.53 μm and also low attenuation at the lasing wavelength around 3.1μm. The feedback fibre has the lowest attenuation at the lasing wavelength to facilitate long optical cavities and, hence, low-repetition-rate pulsed lasing when we implement in the laser system later. The properties of hollow core fibres used in the experiments are summarised in Table 6.

Table 6 Properties of the hollow core fibres employed in this thesis.

	Gain fibre	Feedback fibre
Outer diameter [μm]	233	357
Core diameter*[μm]	109	95
Length used [m]	10	100
Attenuation at 3.1 μm [dB/m]	0.11	0.025
Transmission window near 3.1 μm [μm]	2.8 – 3.5	2.9 – 3.9
Attenuation at 1.53 μm [dB/m]	0.10	-
Transmission window near 1.53 μm [μm]	1.36 –1.56	-

∗ Core diameter is defined as the diameter of the circle inscribing core walls.

CHAPTER 4

4.1 Optically Pumped Gas-Filled Hollow-Core Fibre Lasers

Gas lasers have been demonstrated to be a proficient method to generate mid-IR emission [21], [24], [25], [97]. By incorporate gas laser in hollow core fibre, we can fully utilize the advantages such as high optical confinement, long effective interaction length, and the possibility of control of the effective gain spectrum make it possible to develop a novel type of laser - fibre gas lasers, which combines the advantages of both fibre and gas lasers [25], [98] as we discussed in previous chapters. In this chapter, we will present the laser architecture of our mid-IR fibre gas laser cavity using low-loss hollow core fibre.

Our work builds on recent research showing how molecular species such as acetylene can provide gain at mid-IR wavelengths at low vapour pressure in a cavity when pumped with nanosecond pulses from an optical parametric converter [25], and how this system transfers into a hollow-core fibre in a single-pass amplified-spontaneous-emission (ASE) configuration [39]. The population inversion of C_2H_2 gas by optical excitation in hollow core fibre was firstly realised in Kagome fibre in 2011 [99]. Later, strong single pass ASE emission around 3.15 μm with 30% power conversion efficiency was achieved in C_2H_2 molecules inside a 10 m HC-fibre pumped by a diode laser at 1.53 μm [10].

A system using acetylene as the gain medium can be pumped using a stabilised, modulated, fibre-amplified diode laser around 1.53 μm [10]. In those experiments, although amplification of spontaneous emissions was enhanced by the waveguiding provided by the fibre, there was no cavity feedback and only pulsed single-pass operation was reported. Pump peak powers of tens of watts were required for appreciable conversion [10], [39] while CW operation was not achieved.

Recently, the CW operation of a different molecular system at 1310 nm was reported [31]. A linear cavity incorporating a short (20 cm) straight hollow fibre placed within a gas cell containing molecular iodine was pumped with a tunable, single frequency, frequency-doubled Nd: YVO$_4$ pump source. Very high fibre attenuation at the pump wavelength (>40 dB/m) was overcome by using only a short fibre length and high gain from a molecular transition with rapid de-excitation of the lower laser level. Based on these previous works, we are demonstrating a continuous wave (CW) and synchronously pumped ring fibre laser cavity of acetylene gas by adding NC-HCF as a feedback fibre. This chapter will first describe the experimental configurations and explained each component in the system. We start with, the description configuration of diode laser for continuous wave (CW) operation.

4.2 Experimental setup

4.2.1   Pump Source

The pump source was derived from a tuneable telecommunications grade CW distributed feedback (DFB) laser diode (*ID Photonics GMBH, CoBrite DX1*, linewidth <100 kHz, maximum output power ~40 mW). Wavelength tuning was achieved with the standard temperature and current stabilisation of the built-in laser driver. The laser was not locked to the molecular absorption, but was tuned to the observed maximum absorption and was found to be sufficiently stable not to require further tuning or stabilisation. When required, the signal from the pump diode was amplified using a laser diode pumped (pump wavelength at 1540 nm, total pump power 460 mW) an erbium-doped gain fibre as shown in Figure 19.
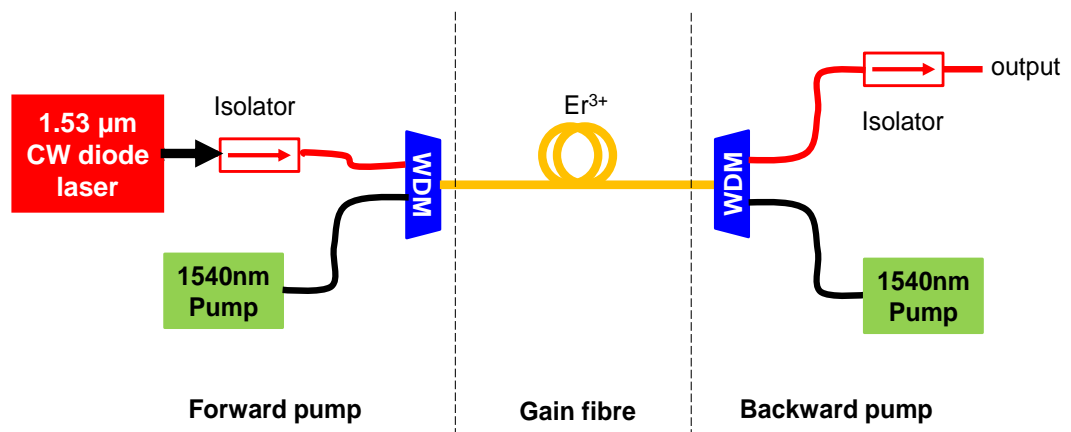
Figure 19 shows the amplified continuous wave diode laser setup. Tunable CW laser, two laser diodes (LDs) provide the pump power for the erbium-doped fibre. The pump light is injected via wavelength-division multiplexing (WDM). The optical isolators reduce the sensitivity of the device to back-reflections.

4.2.1.1 Erbium-doped fibre amplifiers

We used EDFA to amplify our signal from the CW DFB laser diode. In this section, we will describe the characteristic of EDFA configuration that applied in this works. In our source pump system, a 2.4 m erbium doped fibre (Thorlabs ER16-8/125) is used as an amplifier, bi-directionally pumped with a 1540 nm laser diode as shown in Figure 19. The erbium doped fibre either can be pumped by 980nm light, in which case it passes through an unstable short lifetime state before rapidly decaying to a quasi-stable state, or by 1540 nm light in which case it is directly excited to the quasi-stable state. A higher power efficiency can be achieved by in-band pumping around 1540 nm. However, stimulated emission by pump light then limits the possible excitation level, hence also the gain per unit length, and the maximum gain occurs at longer wavelengths.The optical isolators are installed in the configuration to protect the optical components and avoid self-excited oscillations in the EDFA.
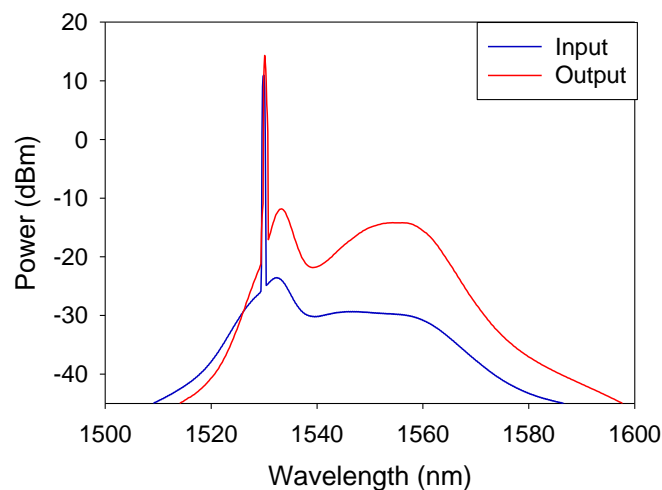
Figure 20 shows measured input and output spectral of the EDFA.

Figure 20 shows measured spectra of the signal input and the output of our EDFA. The gain of 3 dB was achieved, and maximum output from the EDFA with bi-directional pump laser is around 70-75 mW. As the technologies are mature and relatively cheap, it is very reliable to use as the pump source for our laser. In this works, the usage of Erbium-doped fibre amplifiers and another optical device, the performance of the diode laser can be improved to higher output power. Moreover, our tunable CW DFB diode laser also can be modulated and/or amplified using telecom technology when required.

4.2.2 Laser architecture
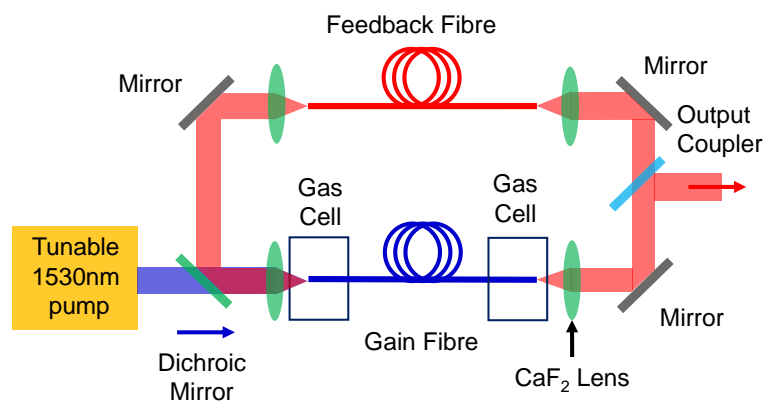
Figure 21 Experimental layout of the laser cavity

The laser setup is shown in Figure 21. The laser system relies on the use of a hollow-core fibre in two ways. The gain fibre (blue) is to confine the light (at both pump and laser wavelengths) and the molecular gain medium simultaneously. The low-loss fibre at the pump and laser wavelength reduced power overlap of the guided mode with the silica core-surround to allow better optical power handling, making it an ideal host for high power gas lasers.
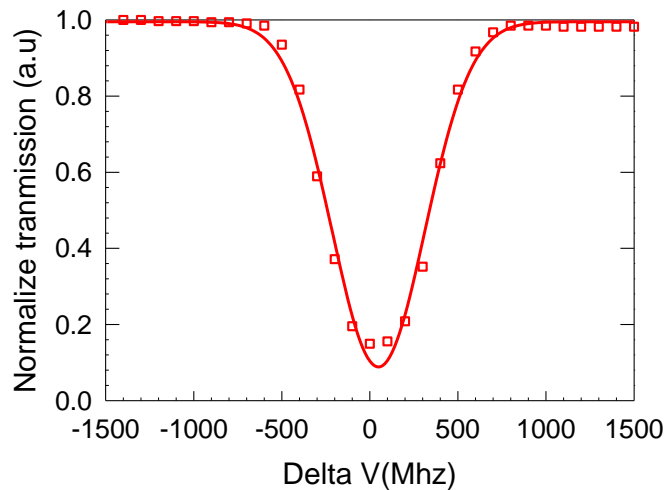
Figure 22 The measured acetylene ($^{12}C_2H_2$) P (9) absorption line measured in 10m gain fibre with 0.25 mbar pressure.

The acetylene pressure in the gas cells was adjusted so as to optimise the laser output power for the acetylene P(9) pump line from the R-branch of acetylene rotational-vibrational absorption spectrum (refer to Figure 7(b)). The data presented here were recorded for a gas pressure of 0.25 mbar as shown in Figure 22. We measured the linewidth of an absorption line to be 613 MHz by tuning our narrowband pump across the transition and measuring the transmitted light. The calculated Doppler broadening linewidth is 480 MHz (for $^{12}C_2H_2$, room temperature, central wavelength 1.53 µm). Acetylene is pumped using a CW distributed feedback diode laser tuned to one of the absorption lines at 1530.383 nm.

The 1530.383 nm pump light was collimated, passed through a custom made a 45º dichroic mirror (transmits 1.53 µm, T > 90 %, reflects 3.1 µm R ~ 99 %) into the cavity. Pump and circulating laser light were then coupled into the gain fibre (10 m length) through an optical window (3 mm thick uncoated sapphire). All fibre coupling lenses were 50mm focal length CaF$_2$ lenses. The pump coupling into the fibre was estimated to be around

80 % which includes lens and gas cell window and the 3.1 μm circulating light coupling was simultaneously estimated to be 60% which includes dichroic mirror, lens and gas cell window. At the output of the gain fibre, the light left the gas cell through an uncoated sapphire window. It was then collimated before passing through the output coupler. At first, about 7% of the total power is coupled out of the cavity using an uncoated CaF_2 window as an output coupler. By using the 7% output coupler, the maximum output power is around 0.4 mW.
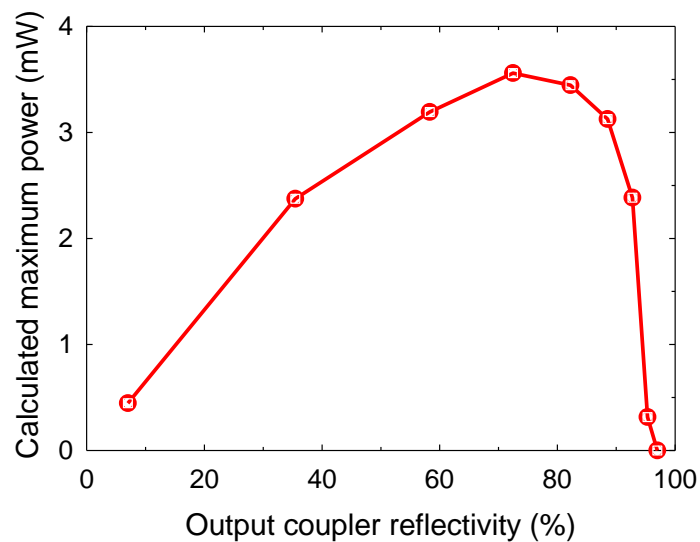
Figure 23 the calculated attainable output is plotted versus output coupler reflectivity (%).

The output power extracted from the cavity could be increased if we optimised the reflectivity of the output coupler. The curve in Figure 23 shows, the potential output power if we vary the reflectivity of the output coupler. This curve is derived from a measurement of the actual output power at a fixed output coupling by an inserting variable attenuator after the output coupler. It shows that we can expect to obtain around 3.5 mW output power from our configuration if we use a 70% output coupler. Two output couplers were employed in this work, one with 70% reflectivity

(chosen to maximise output power) and an output coupler with 7% reflectivity. The laser light transmitted through the output coupler was then coupled into the feedback fibre with an estimated efficiency of 75 %, and the output was recombined with the pump on the dichroic and coupled back into the gain fibre.

4.2.3 Laser cavity

The laser cavity is a vital component in a laser system. A laser requires a laser cavity or laser resonator, in which the laser radiation can circulate and pass a gain medium which compensates the optical losses. The laser cavity or laser resonator typically is an arrangement of mirrors that form a standing wave cavity resonator for light waves which called linear cavity/resonator.

Linear (or standing-wave) resonators are made such that the light bounces back and forth between two end mirrors. For continuously circulating light, there are always counter-propagating waves, which interfere with each other to form a standing-wave pattern. There are also have ring cavity type. In the ring cavity/resonator, light can circulate in two different directions. A ring resonator has no end mirrors.

Compared to linear cavities laser, ring lasers have certain properties that make them useful for a number of applications. The round trip dispersion caused by the active medium in ring laser is half of that in a linear laser since the pulse travels only once per round trip in the active medium in ring laser. The thermal properties of such lasers are also better for the same reason, which reduce the losses associated with thermally induced aberrations. In addition, more stored energy in the active medium could

be obtained because of the absence of the effect of spatial hole burning in a travelling-wave ring laser. Consequently, an optical ring cavity which is inherently stable.

In this work, we choose the ring cavity rather than linear cavity simply because in our synchronously pump laser operation, the laser system needs a long optical cavity to facilitate a delay time for the acetylene molecules to depopulate to the ground state in order to start the lasing. As we discussed in Chapter 2, the acetylene lower laser state is forbidden dipole to ground state, means the acetylene molecules cannot go to ground state only by intermolecular collisions or molecules-core wall collisions. The other reason to used ring cavity because of the practicality and easier when doing an alignment compared to the linear cavity.

We used the hollow core fibre with low attenuation at the laser wavelength as a feedback fibre. The feedback fibre will feed the laser light back into the gain fibre and complete one round trip cavity. By feeding back the laser light multiple time passing through the gain fibre, the laser light will be amplified each time.

4.2.4 Alignment of cavity laser

In our system, the ring laser cavity is formed of two hollow core fibres and some additional elements. Precise alignment is needed when assembling an optical cavity. For best output power, optical elements must be aligned such that the path followed by the beam is centred on each item. Lenses and mirrors are used to achieve high coupling efficiency from one fibre to the other at the lasing wavelengths (3.12 to 3.16 µm). This coupling is often difficult due to the critical alignment of optical components. The mid-IR light cannot be seen by human eyes, and there is no viewer that we can use in the alignment process.

Figure 24 shows a ring laser cavity with tunable pump source, two hollow core fibres, three mirrors, M1, M2, M3, one dichroic mirror, lenses and an output coupler. The three mirrors and dichroic mirrors are all completely reflecting optical beams having a wavelength of 3.16 µm. Before aligning the ring cavity, the 1.53 µm pump light was collimated, passed through a custom made dichroic mirror into the gain fibre as shown in Figure 24 (a). The pump coupling into the gain fibre was estimated to be around 80 % which includes lens and gas cell window. The alignment of ring cavity was carried out in two stages. For initial alignment, a CW HeNe laser at 3.39 µm (*Thorlabs H339P2*, average power ~ 2 mW) was used as a reference laser. The CW HeNe laser was coupled into feedback fibre using lens, mirror M and mirror M3. Mirror M is for alignment only and is not a part of the ring cavity. The 3.39 µm light from feedback fibre was used to align the mirror M1 and dichroic mirror to couple back into the gain fibre as shown in Figure 24 (b).
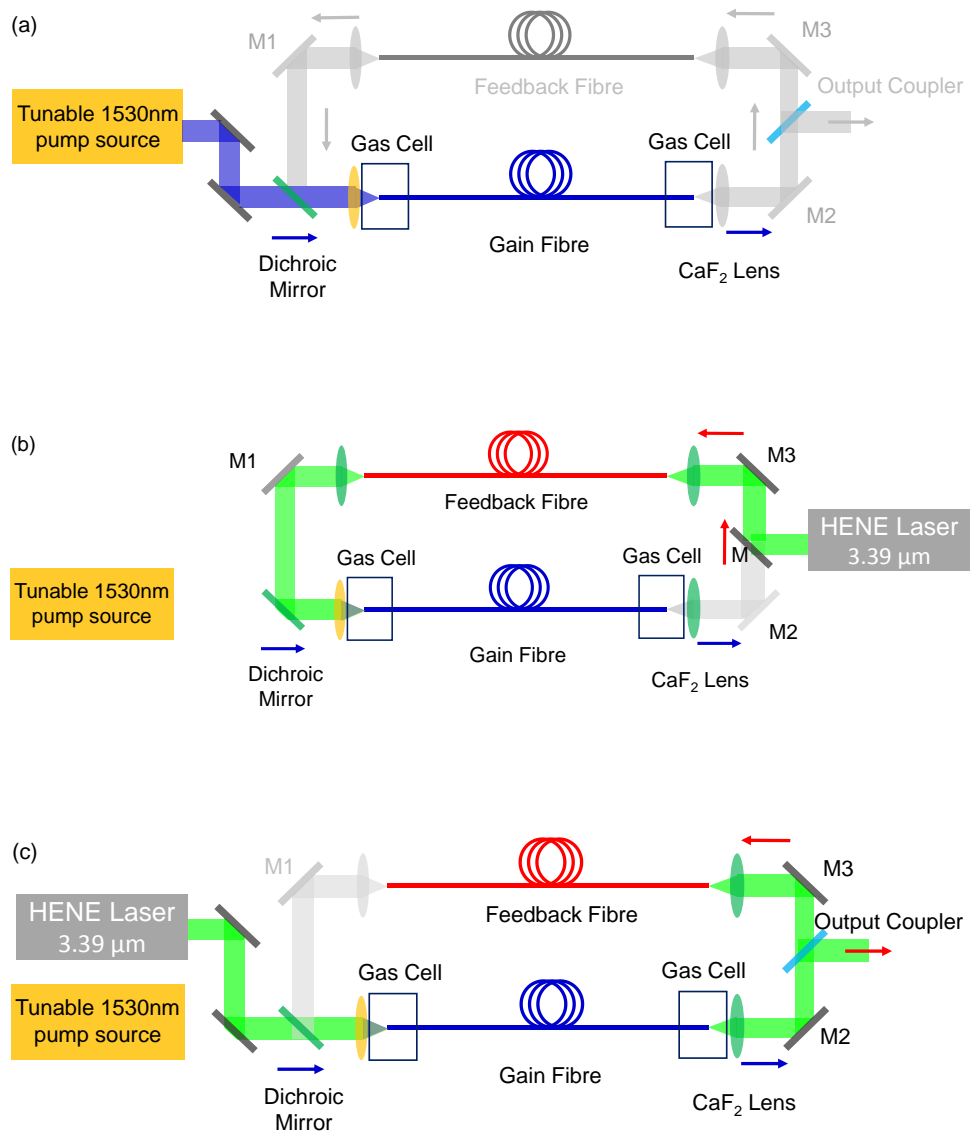
Figure 24 shows the laser cavity alignment processes. It starts with (a) couple the 1.53 um pump source into gain fibre. In this step, the dichroic mirror is place and fix in between pump source and the gain fibre. The seconds step (b), 3.39 μm light from HeNe laser was coupled into feedback fibre; the light come out from feedback fibre used to align mirror 1 and dichroic mirror so that 3.39 μm light can couple back into the gain fibre. Last (c), 3.39 μm light coupled into the gain fibre to align mirror 2 and mirror 3 to feed light into feedback fibre.

In the second stage of alignment, reference laser light was passed through the gain fibre and coupled into feedback fibre to align mirror M2 and mirror M3. In Figure 24(c), mirrors, M2 to M3, are carefully positioned to couple the light back into feedback fibre. However, due to the offset of the wavelength of HeNe laser from the acetylene laser, the coupling efficiency then needed to be further optimised for the lasing wavelengths by pumping the laser and monitoring the output power. The 3.1 μm circulating light coupling was simultaneously estimated to be 60 % which includes dichroic mirror, lens and gas cell window.

4.3 Summary

In this chapter, we presented our fibre gas laser configuration and explained each component in the system. We also demonstrated the alignment technique that we used to obtain the ring cavity to enable the laser system works. The precision of cavity laser alignment help to reduce loss in the cavity laser system and allow the laser system operate in low pump threshold. In the next chapter, we will discuss more results that we obtained in the continuous wave (CW) and pulsed operation.

CHAPTER 5

5.1 CW Lasing of Mid-infrared Acetylene Gas Hollow Core Fibre Laser

Following the description of the configuration of a new form of mid-infrared fibre laser presented in Chapter 4. We introduced the experimental work and analysis of CW lasing of the mid-infrared hollow core fibre gas laser. The continuous wave (CW) lasing of mid-IR hollow core fibre gas laser based on population inversion remained elusive. CW operation of an acetylene laser is made harder by the lack of a radiative transition from the lower lasing levels. The requirement for a non-radiative (collisional) de-excitation pathway affects the laser dynamics and limits the efficiency [100].

The motivation of the continuous wave (CW) operation came from the synchronous pump operation that we will discuss in Chapter 6. In the pulse operation, while us sweeping the pump repetition rate to the lower repetition rates. Unexpectedly, the output power of the laser continues increased. As the results, we removed the modulator (generating pulse) from pump source system and try to operate the laser system in the continuous wave operation. The experimental and numerical results of CW mid-IR hollow core fibre gas laser will be discussed in this chapter.

5.1.1 CW laser configuration

The experiment configuration of the CW laser was described in chapter 4. Acetylene is pumped using a CW distributed feedback diode laser tuned to one of the absorption lines of acetylene around 1530 nm. In operation, the pump was tuned to one of the acetylene P-branch absorption lines around 1530 nm. With a feedback fibre length of 3 m, we then detected lasing at corresponding transitions around 3.1 μm. As we mention earlier, our feedback fibre has low attenuation at laser wavelength around 0.025 dB/m. By using a short piece of feedback fibre provides the lowest loss for the feedback system. The acetylene gas pressure and the length of the gain fibre need to be adjusted to achieve optimum output laser.
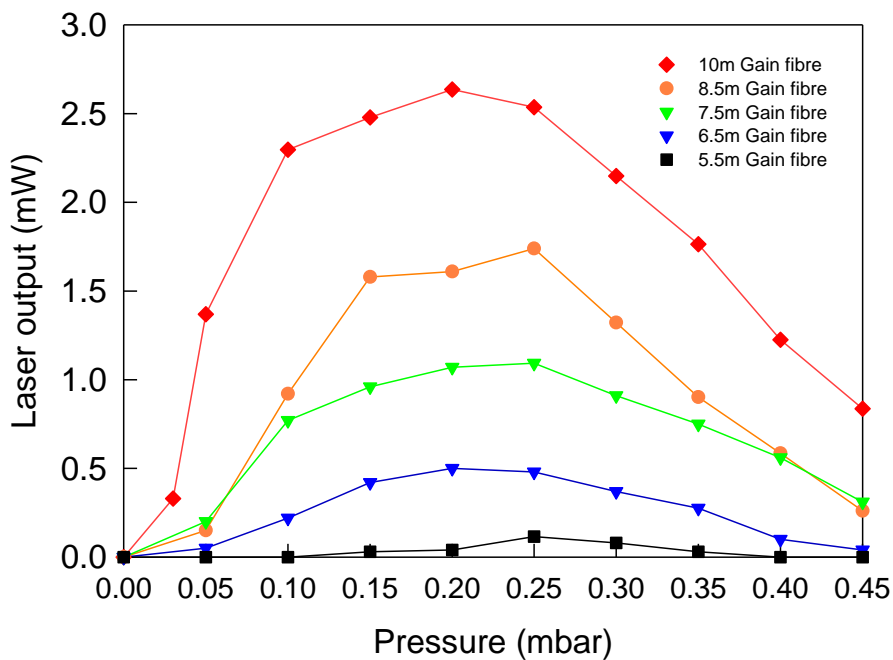
Figure 25 shows optimisation of the pressure for several lengths tested of gain fibre.

The various gain fibre length is tested for optimisation of pressure in the fibre to maximise the output laser as shown in Figure 25. By using different

gain fibre lengths, we found that 10 m gave the best laser performance at the 0.25 mbar pressure. The lowest output power measured is 0.02 mW at 0.25 mbar when we used 5.5 m length gain fibre. When using the gain fibre length below than 5.5 m length, our pump pulse energies do not produce measurable emissions. The lowest output when we shorten the gain fibre length because broadening loss and others factor dominates the gain generated in the gain fibre. As the acetylene pressure increases from zero, the increasing molecular density in the gain fibre results in more pump absorption and gain, giving higher CW lasing output. Increasing pressure also results in more rapid rovibrational energy transfer processes. Beyond a certain pressure, when intermolecular collisions dominate over inelastic molecule-core wall collision, the transition rate from the laser lower level to ground level will be significantly reduced. Lasing would be reduced and will eventually stop as the gain is reduced. A similar trend of output power dependence of pressure was also found in the single ASE measurement [10].

Figure 26(a) shows the normalised measurement of CW lasing for different pump lines. For CW pumping (Figure 26(a)) we typically observed two lines arising from the $\Delta J = \pm 1$ transitions from the common upper level populated by the pump excitation. For each pump transition, the $\Delta J = \pm 1$ laser transitions share a common upper level [35] and so are in competition, and one might expect to observe just a single line above the threshold. However, the gain for the above-threshold line is reduced as the population builds up in its lower lasing level until it is exceeded by the gain provided to the competing line (with a lower lasing level which is still empty), allowing this second line to lase as well. Thus, broadly up to half of the pump photons can result in a laser photon for the highest-gain

line, and up to half of the remainder may lead to a photon on the second line.

a)

b)
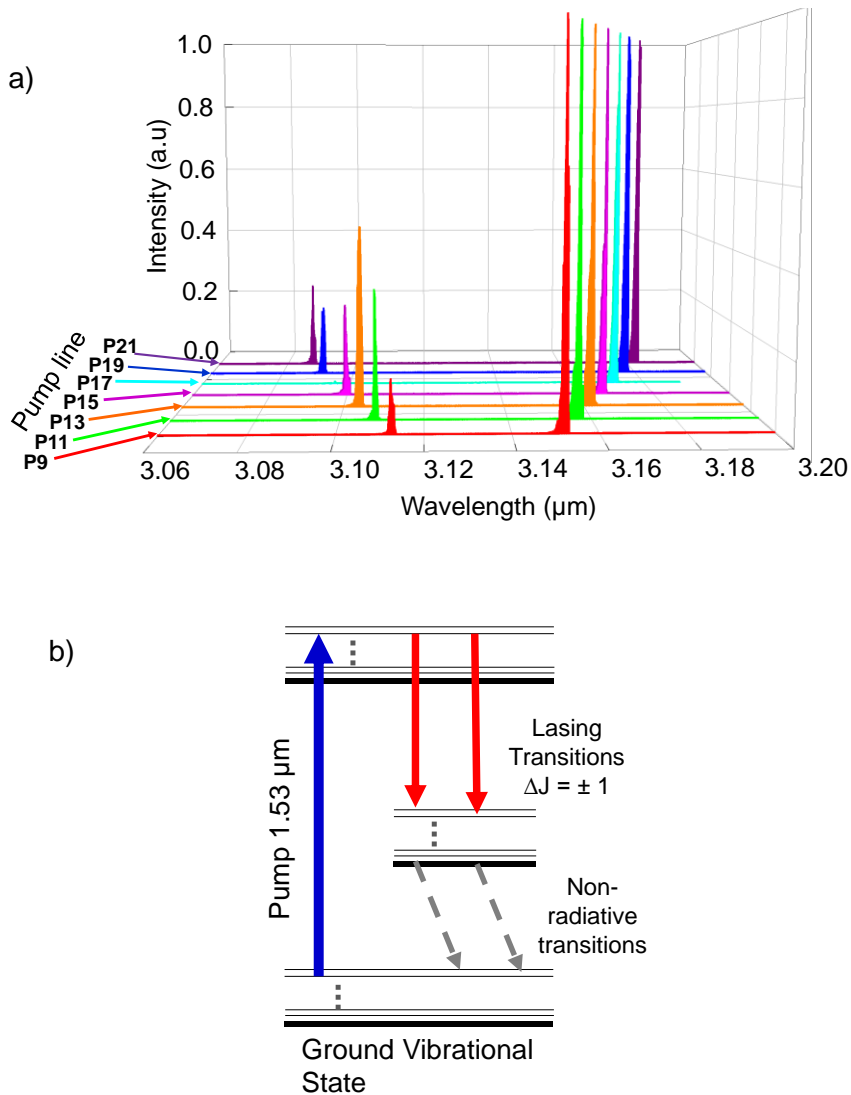
Figure 26 CW lasing by acetylene. (a) Measured optical spectra for different pump transitions (resolution 1 nm). The (b) Selected acetylene molecular energy levels, showing the radiative transitions involved in lasing. Note that there is no radiative transition from the lower laser level to the ground state.

The two peaks (red line) correspond to transitions from the $J = 8$, $v_1 + v_3$ excited state to the $J = 7$ in branch R and $J=9$ in branch P, v_1 state. The divergence in the shift of the two transitions be influenced by two different branches (R and P branch) in rovibrational acetylene absorption spectrum (see Figure 7(a)). As we tune to longer wavelength pump line in P branch

71

and the second laser line will excite in shorter wavelength pump in R branch. For CW operation, a fast repopulation of the ground level and depopulation of the lower lasing level are usually required for the laser medium. However, in acetylene, the transition from vibrational state to the ground state is dipole forbidden. Details of the transition routes remain unclear. The inelastic collision between acetylene molecules and core fibre wall can help depopulate both upper and lower laser levels, which may be crucial for the sustainability of CW lasing. Meanwhile, rapid rotational relaxations may also participate in CW lasing operation and play a major role by rotational energy transfer process [101].
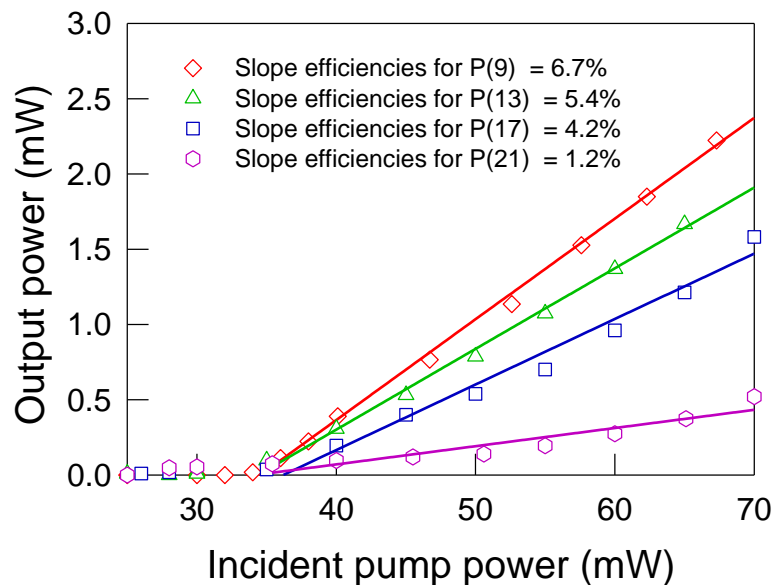
Figure 27 Slope efficiencies of total power at 3 μm for different pump lines when acetylene pressure was 0.25 mbar under room temperature.

The measured pump power versus power output curve for pumping at 1.53 μm for various pump lines when acetylene pressure was 0.25 mbar under room temperature is shown in Figure 27. Highest output powers are

obtained using 70% output coupler when P(9), which has the maximum absorption cross-section in the P-branch, is pumped. Under CW pumping our cavity oscillated bi-directionally, with slope efficiency 6.7% (single output measured). As we tuned the pump line to higher P-branch, the slope efficiency has gradually decreased. This corresponds to the strength of the absorption line of the acetylene as we can refer from the HITRAN data [102]. The slope efficiency for another pump line P (13), P (17) and P (21) line was 5.4%, 4.2 % and 1.2% respectively. Note that although the laser oscillates bi-directionally, only one of the outputs is measured here. No saturation of the output power was observed as we increased the pump power to the maximum (75 mW). The incident pump power is measured before coupling into the fibre, and the 3 μm output is measured after coupling out by the output coupler. The pump coupling efficiency is 80%.

Note that, the slope efficiency drops as we tuned to higher pump line in the P-branch but the incident pump threshold for all pump line is almost the same value. In Figure 27, the measured pump threshold for all measured pump line at a pressure of 0.25 mbar is around 35 mW incident pump power. To reduce the threshold, we have used a lower output coupling of 7 %. A reduced pump threshold of 16 mW then enables our cavity to lase when pumped directly by our unamplified pump laser, although with reduced efficiency. This configuration is ideal to be used as a seed in a possible oscillator/amplifier configuration, with overall amplifier efficiency expected to be ~ 20% [10].

5.1.2 Numerical result

The simulation model of the calculated pump threshold with acetylene pressure from the acetylene-filled hollow-core fibre laser was carried out using simple rate equations as discuss in Chapter 2. The model predicts the behaviour of the incident pump threshold versus the pressure of acetylene in the gain fibre. The measured and calculated incident pump threshold as a function of acetylene pressure are shown in Figure 28.

In Figure 28, the numerical model shows the same overall trends that are seen in the experimental data showing a quadratic trend. When we increase the acetylene pressure, the incident pumps threshold of the laser decrease to the minimum pressure. Beyond the minimum pressure, the incident pump threshold is increased back. The lowest incident pump threshold for the experimental value is 22 mW at 0.20 mbar, which is slightly lower for the calculated value is 18 mW at 0.35 mbar using the model.

Based on the rate equations in Chapter 2, the number density of the acetylene molecules, N can be computed by using ideal gas law as,

$$N = (pV)/k_B T \qquad (21)$$

where p is the gas pressure, k_B is the Boltzmann constant, V is the volume of the acetylene gas and T is the temperature of the gas (room temperature in this case). The gas pressure controls the number density of the acetylene molecules in the gain fibre. By increasing the gas pressure, means more density of molecules in the ground state. Thus, increase the chances to achieve the population inversion until up to the

certain point where pressure broadening (and other losses) dominate the gain. The minimum pressure essentially occurs when a given pump power creates just enough gain by the end of the fibre to balance the fibre loss.

After the minimum pressure, any further increase in pressure causes additional pump absorption, resulting in a reduction of the gain to below the fibre loss and also decrease the upper-level state lifetime, τ. The interplay of both effects, play an important role causing the increasing in the incident pump threshold at high pressures as shown in Figure 28.
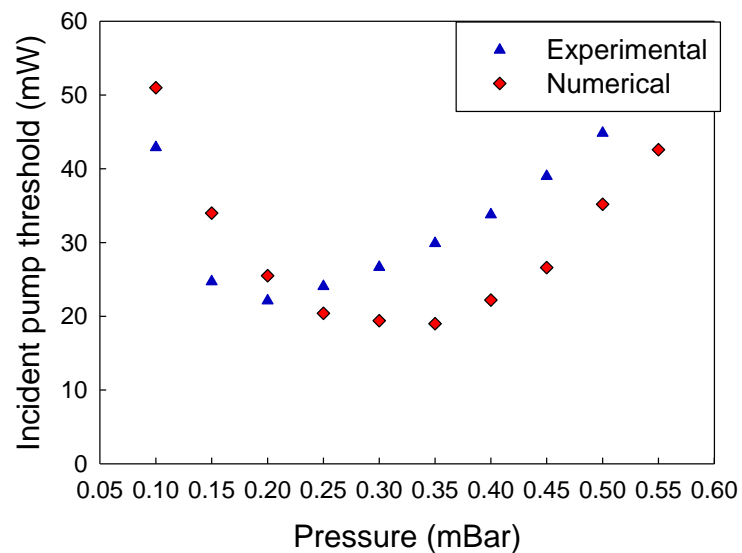
Figure 28 Experimental and calculated incident pumps threshold as a function of acetylene pressure.

5.1.3 Stability of the cavity laser
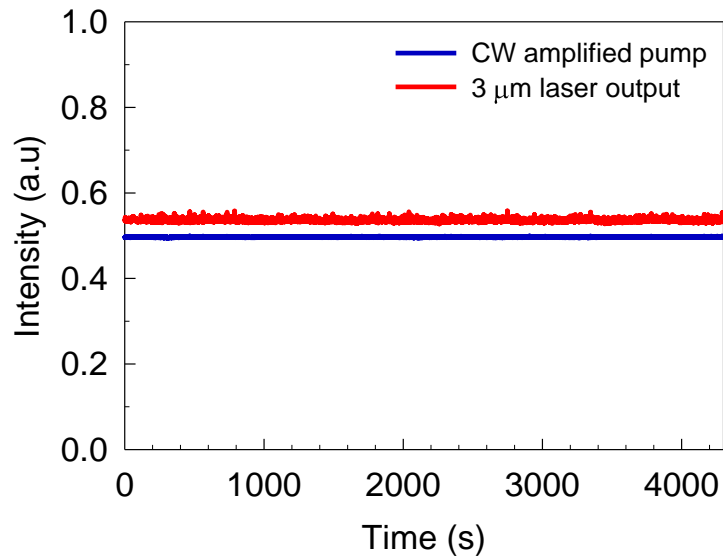
Figure 29 shows the excellent stability of the laser over long time scales.

The stability of laser cavity depends on how good the alignment of the cavity laser itself and affect the beam quality of the laser. Figure 29 shows the stability of the CW laser output as a function of time. The stability of CW laser output as a function of time measured at 10 Hz over more than 1 hour. Note that, apart from the standard stabilisation of the pump laser diodes; there is no frequency locking of the pump, or stabilisation or acoustic isolation of the laser cavity. The pump power was 75 mW on the P(9) transition. The pressure of acetylene gas was 0.25 mbar. 70% output coupler was used and the output power was about 2.5 mW. A high gain detector (*Thorlab PDA20H-EC*) was used to measure the lasing power directly.

5.1.4 Mode profile of a mid-IR fibre gas laser

A laser beam quality defines aspects of the beam illumination pattern and the merits of a particular laser beam propagation and transformation properties. A typical measure of the quality of an optical beam is the M^2 parameter [103]. The description of "quality" also depends on the application. While a high-quality single-mode Gaussian beam (M^2 close to unity) is optimum for many applications in the area of laser material processing, printing, marking, cutting and drilling. For laser surgery, a uniform multimode top-hat beam intensity distribution is required [104].
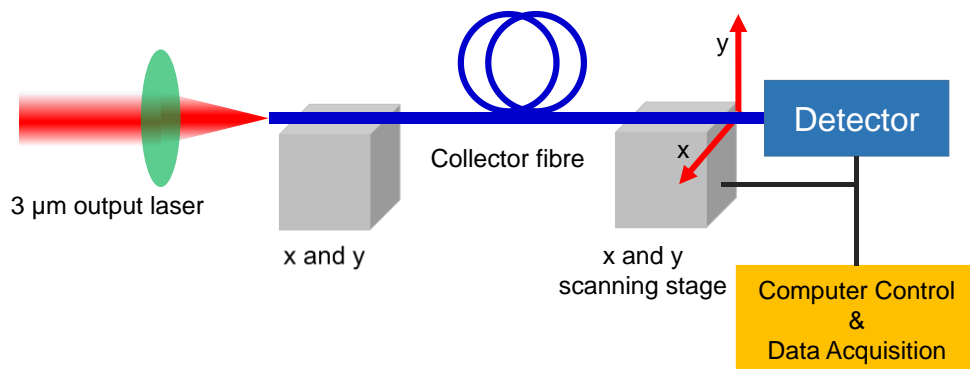
Figure 30 Schematic of the beam profile imaging. The 3 μm laser picked off from the laser cavity by output coupler and collimate into probe fibre.

Here in this work, we do not measure the beam profile using the M^2 technique. What we did is measuring and recording using a two-dimensional scan across the output beam. We acknowledge the help of Ms Mengrong Xu in recording the 2D scan of the mode pattern. The schematic experiment layout is shown in Figure 30. The 3 μm light picked off from a laser cavity is coupled into the probe fibre. Here, the passively guided output mode was imaged onto an InSb array by placing the fibre end as close to the array input window as possible. The probe fibre is

positioned on automated translation stages to move the fibre end in x and y directions perpendicular to the beam propagation direction. The probe fibre is scanned in x and y with 0.1 µm step size, and at each (x, y) point the detector is measured. Computer control is used to automate the movement of the fibre probe and acquisition of the detector. The transverse profile and 2-D and the 3-D beam profile from this measurement are plotted in Figure 31. An image of the 3.1 µm wavelength mode profile from the fibre gas laser is shown in Figure 31. The mode shows reasonably good azimuthal symmetry. This measurement is the initial step toward understanding and examines the beam quality from our fibre gas lasers.
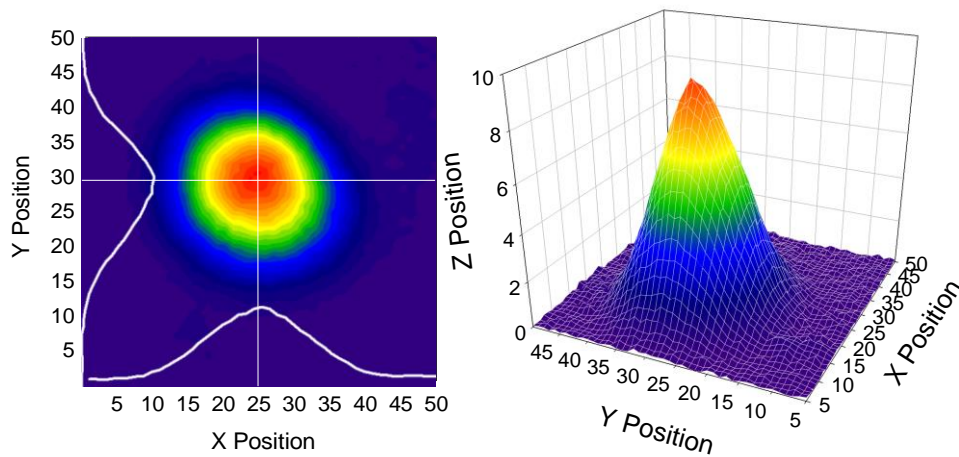
Figure 31 shows the mode profile, measured using a two-dimensional scan across the output beam and plotted into the 3D plot.

Figure 31 shows the high beam quality of the laser output in 2D and 3D view. From the 2D view of the beam enables us to see the entire beam simultaneously. From the transverse plot, the uniformity of our beam profile can be determined. As we can see, our laser beam has a Gaussian beam profile. A Gaussian beam allows the highest concentration of focused light. It must be emphasised that the beam profiles observed in these experiments are very stable. This measurement is the initial step toward understanding and improving beam quality from gas-filled hollow-core fibre lasers.

CHAPTER 6

6.1 Synchronously Pumped Mid-IR Hollow Core Fibre Gas Laser

The first demonstration of laser emissions from population inversion in an acetylene gas-filled HC-PCF was in 2010 by Dr Rudolph's group at New Mexico [25]. Previous works [26], [31], [32] has shown that single-pass amplified spontaneous emission (ASE) can lead to a measurable output from this transition but continuous-wave laser operation is not possible because of the fact that the lower laser level cannot spontaneously transit back to the ground state. As a result, the laser emission is self-terminating. With the development of the low loss hollow-core fibre (HC-fibre) in the mid-IR region as we describe in Chapter 3, allowing us to use it as a feedback fibre in our laser system. We have used the very low attenuation of our hollow fibres (less 30dB/km at the laser wavelength) to delay the pulse laser output so as to enable the acetylene molecules to return to the ground state through collisions with each other and with the fibre core walls.

Here, we will describe and demonstrate synchronously pumped acetylene fibre laser based on low-loss silica hollow-core fibre. We describe the measurement done, results and analysis from the pulsed laser operation in the following section. Based from the results in the pulse operations, we realise that we can generate CW lasing of mid-IR acetylene gas fibre laser as described in Chapter 5.

6.1.1 Experiment configuration: Synchronously pumped

Pulsed operation of lasers refers to optical power appears in pulses of some duration at some repetition rate. By using modulated, amplified tunable pump diode laser to generate pulse laser from our molecular gas-filled hollow-core fibres laser. Here, we describe how to generate the modulated, amplified signal from CW DFB diode laser.
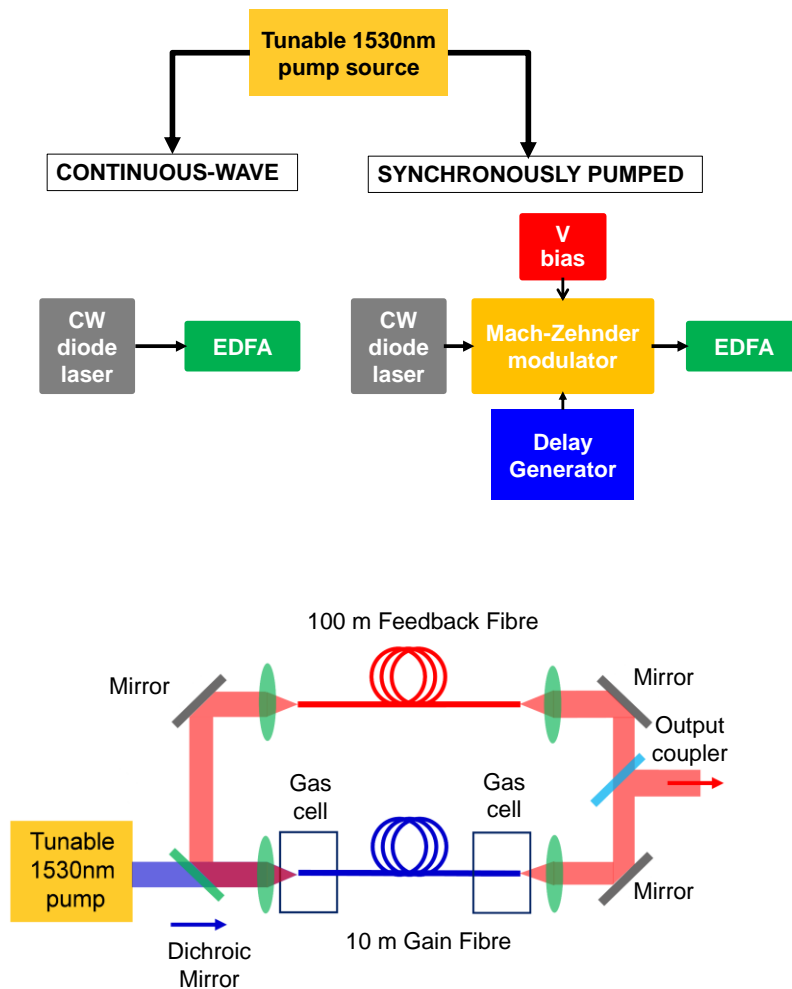
Figure 32 shows we can operate the pump laser in two operations; continuous wave (CW) and pulsed operation. For pulsed operation, the pump repetition rate is carefully adjusted digital delay generator to control the pump modulator so that the circulating laser pulse is coincident in time with the 1.53 μm pump pulse.

For pulsed laser operation, the diode output was modulated before amplification, using a Mach-Zehnder intensity modulator (*Thorlabs LN56S-FC, 10 GHz*) driven by a delay generator (*Stanford Research Systems DG 645*), as shown in Figure 32. It was then amplified to an average power of 72.3mW (pulse energy up to 28nJ) using an EDFA and coupled into the gain fibre through a window.

The ends of the 10 metres long gain fibre are sealed in gas cells; the fibre is evacuated, and then filled with 0.25 mbar of $^{12}C_2H_2$. The mid-IR hollow core fibre gas laser configuration is shown in Figure 32. A pump wavelength of 1530.383 nm from a narrowband tunable diode laser (tuned to an acetylene absorption line) was modulated to 80 ns pulses at a repetition rate of 2.6 MHz, corresponding to the cavity round-trip time. Mid-IR emission from the output end of the gain fibre was coupled into 100 metres length of low-loss feedback NC-HCF.

By replacing the feedback fibre with a longer fibre, the NC-HCF is used as part of a ring cavity configuration to facilitate cavity alignment. A longer length allows pulsed operation at a relatively low repetition rate. In pulse operation, the low-loss feedback fibre used to delay the pulsed laser output so as to enable the molecules to return to the ground state through collisions with each other and with the fibre core walls. When the delayed pulse is fed back into the gain fibre, and it is synchronously pumped this enables pulsed operation of the laser cavity.

We estimate the total feedback loss (including the output coupling) to be -5.9 dB. The pump repetition rate must be carefully adjusted so that the circulating laser pulse is coincident in time with a 1.5 µm pump pulse.

About 70% of the total power is coupled out of the cavity per round trip using a coated custom-made optical component, as the output coupler.

6.2 Pulse laser operation

6.2.1 Experimental results
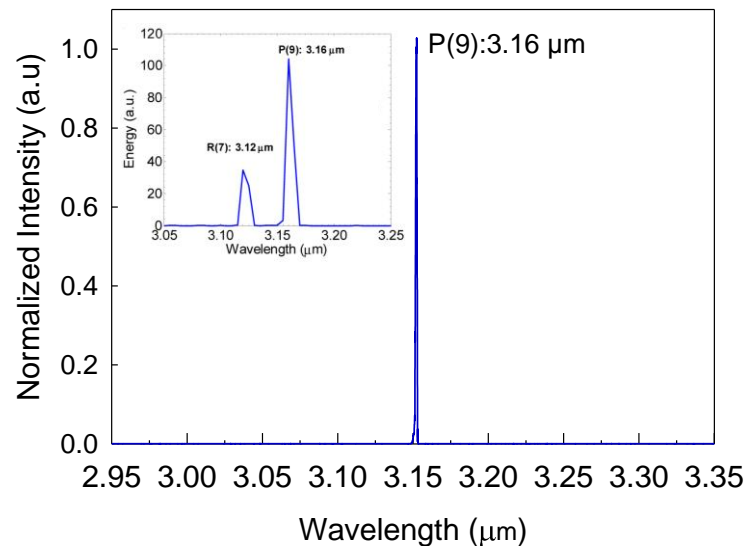
Figure 33 Measured optical spectrum at 0.25 mbar C$_2$H$_2$; the inset shows the optical spectrum reported in [10] **(recorded at low resolution) indicating the presence of two transitions in the ASE mode.**

The output spectrum of our laser is provided in Figure 33. It shows a single laser line at a wavelength of 3.16 µm. The inset shows the output spectrum reported in [10] of the acetylene filled HC-PCF in the single-pass configuration. The single-pass configuration reported in [39], [106] shows two ASE emission lines corresponding to the R (7) and P (9) transitions. In the cavity configuration, only one lasing line is observed above

threshold near 3.16 μm, corresponding to the P (9) transition. This is to be expected because the two lines share a common upper level, and the presence of a single line above the threshold is clear evidence of the effect of feedback in our cavity.

To make the cavity oscillate and lase, we carefully tuned the pump repetition rate by using a *Stanford Digital Delay Generator DG645* to synchronise the circulating laser pulse with a 1.53 μm pump pulse. Oscillations on the pump pulse seen in Figure 34. Maximum output power is recorded when the repetition rate is at the frequency of the ring cavity (2.6 MHz—synchronous pumping). A strong dependence of the 3.1 μm laser output on the repetition rate. When the pump repetition rate is changed, the lasing continues, although with reduced efficiency and stability. We measured and recorded the output power as a function of repetition rate start from 10 KHz up to 5.5 MHz.

In Figure 34, we showed a few laser spectra for single pass configuration and cavity configuration at different repetition rates. Firstly, we look at the point 6, circulating laser pulse with a 1.53 μm pump pulse are synchronise together. The maximum output power is recorded when the repetition rate is at the frequency of the ring cavity (2.6 MHz - synchronous pumping). At point 5 and above, there are no single pass ASE laser spectra detected (see red plotted line).In the absence of feedback, our pump pulse energies do not produce measurable emissions. Indeed, if we block the feedback in our system no output can be measured, and our pump pulse energies are at least 100 times below those used in [39], [106].

The point 8 is the sub-harmonic peak for the ring cavity frequency. The point 2, 3 and 4 are the harmonic peaks. The laser power recovers around harmonic and sub-harmonic repetition rates. At low repetition rates (below cavity frequency), the lasing continues in this region because the pump pulses energy increases at fixed pump amplifier current.
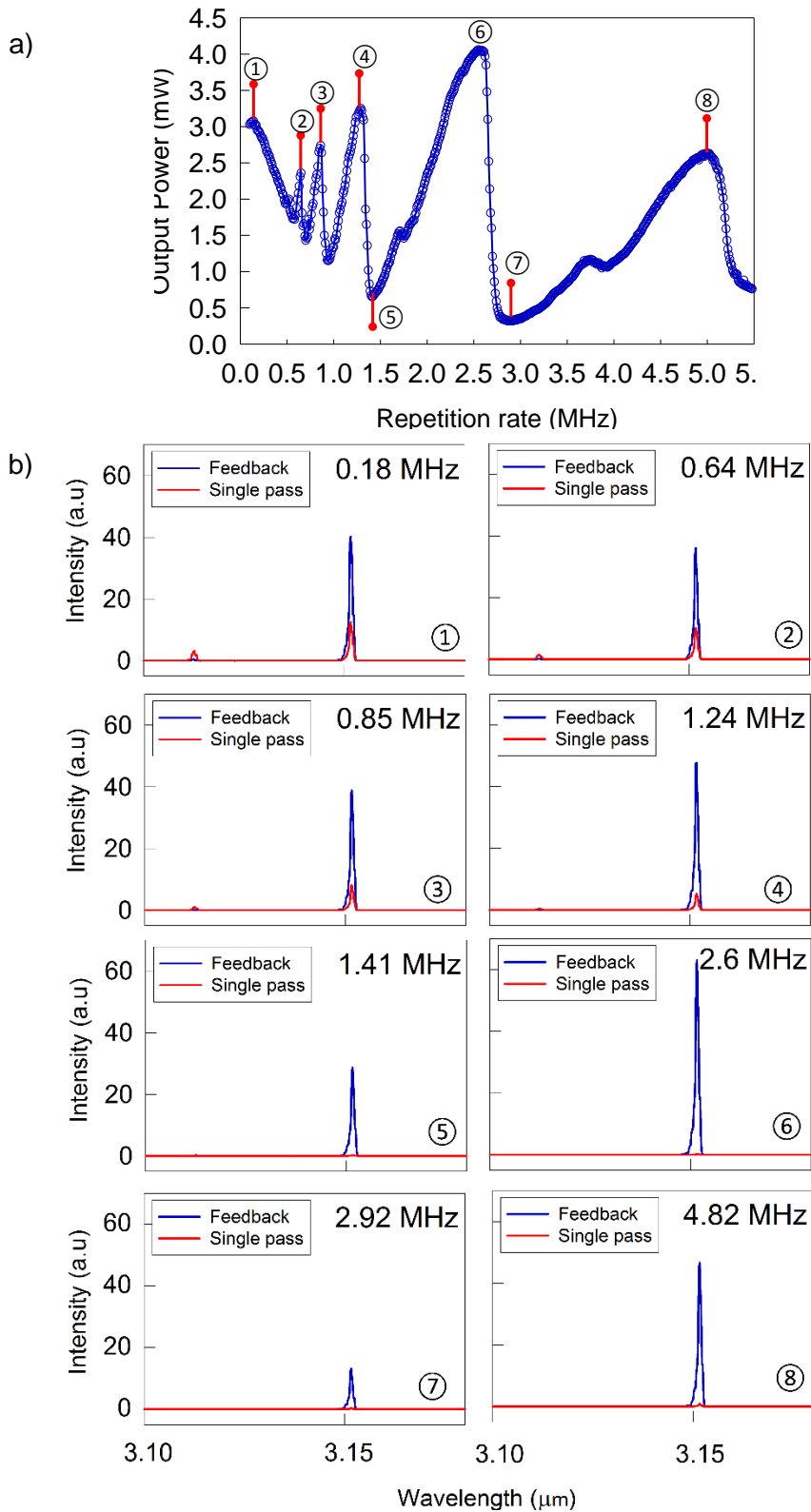
Figure 34 (a) Pulsed lasing by acetylene. Measured output power as a function of pump repetition rate. (b).The recorded spectra show both ASE emission spectra (red line) and cavity configuration (blue line).

As the pump repetition rate is reduced (but without adjusting amplifier pumps) to the point 1, the pump pulse energy increases and less feedback is required to generate a detectable output, resulting in less sensitivity to the pump repetition rate as we approach the single-pass amplified spontaneous emission (ASE) regime. As we can see in the recorded spectra, both configuration single pass emission (red line) and cavity configuration (blue line) can operate in this region.

However, we still are unable to detect an output under any circumstances when the feedback is blocked because even at these lower repetition rates (0.1MHz), the pump peak powers (5.8 W) and pulse energies (0.46 µJ) are much lower than in previous single pass ASE experiments [10]. There is a rapid decrease in the output when increasing the repetition rate above the cavity frequency. This behaviour indicates the decay of the excited state is rapid even at low pulse energies. Spectrally, the output when synchronously pumped is dominated by a single strong line, with only the weak detection of a second line.

Based on that observation, it leads to the initial idea to replace the laser system with continuous wave (CW) pump source to generate the CW lasing in mid-IR wavelength as we discussed in Chapter 5. All spectral measurements were performed using a 300 mm focal length scanning spectrometer (*Bentham Instruments TMc300*) fitted with a 300 lines/mm grating and a liquid-nitrogen-cooled InAs detector (*Electro-Optical Systems S-010-LN4*). The resolution used was 1 nm.
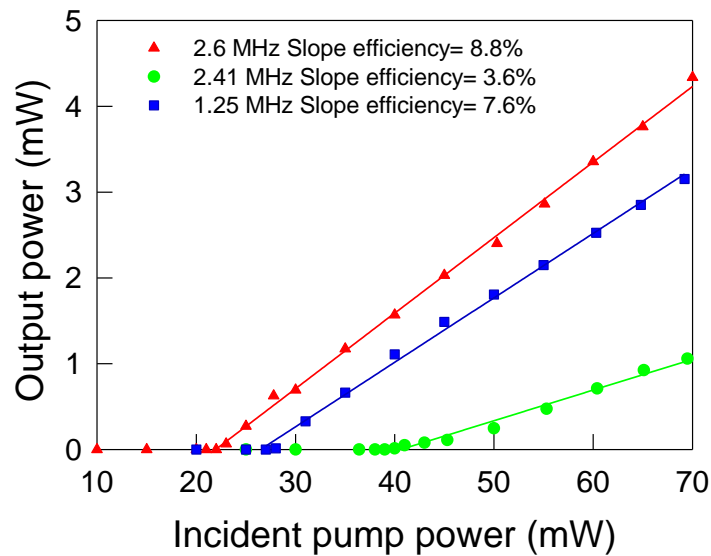
Figure 35 Pump power–output power curves for selected repetition rates. The slope efficiency at synchronous pumping (2.6 MHz)) is 8.8%, with just one spectral line lasing.

The measured selected pump power–output power curve for pumping at 1.53 μm at different repetition rate when the C_2H_2 pressure was 0.25 mbar under room temperature. When the pump repetition rate is not at harmonic and sub-harmonic frequencies of the cavity, the efficiency of lasing output is quickly reduced. Using an average pump power of tens of milliwatts (peak power <100mW at 2.6 MHz) we easily reach threshold for laser oscillation under pulsed pumping and our cavity oscillates with a slope efficiency of 8.8 %, where at sub-harmonic peak (1.25 MHz) the slope efficiency is 7.6% and at 2.14 MHz repetition rate (the lowest point before the repetition rate reach cavity frequency- see figure) the slope efficiency is 3.6% as shown in Figure 35. When the repetition rate is at the frequency of the ring cavity (2.6MHz) the incident pump threshold is recorded around 23 mW. The pump threshold is increasing when the repetition rate is not at a frequency of the ring cavity.

By using 7% of the output coupler, the threshold pump power can be reduced to below 20 mW. The threshold value of the incident pump power to obtain a 3.16 μm output is around 16 mW. Obviously, it also reduces the laser output power. By using the 7% output coupler, the recorded output power is around 0.4 mW when the incident pump power is 37 mW as shown in Figure 36. The slope efficiency is only 2%.
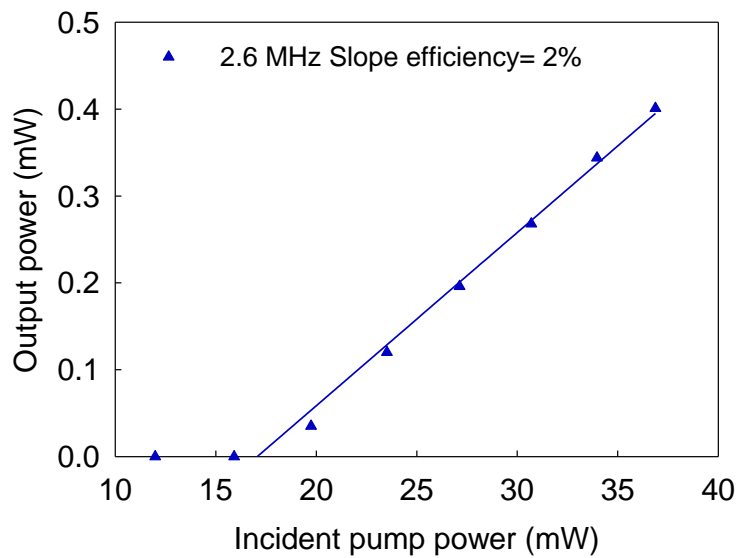
Figure 36 Measured output power (blue triangles) measured after output coupler is plotted versus the incident pump power at 0.25 mbar pressure

Emissions from the system when synchronously pumped take the form of a pulse train emitted at the round-trip repetition rate of the laser cavity and correspond to copies of a single pulse circulating inside the cavity. All the pump powers were measured after the dichroic mirror and before the input lens and window. Measurements of optical powers were performed using a thermal power metre (*Ophir 3A-SH*).

6.2.2   RF and time-dependent measurements
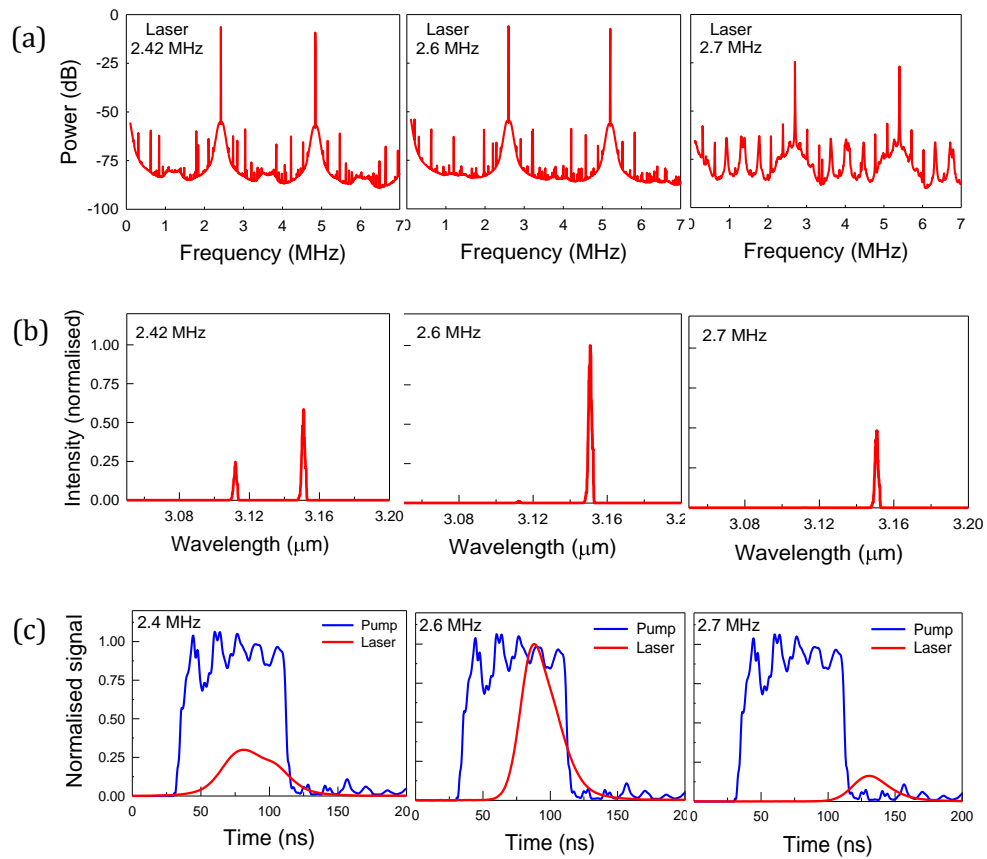
Figure 37 (a) RF spectra, (b) optical spectra, and (c) time dependence for the pump (blue) and the laser (red) at selected repetition rates spanning the peak performance in Figure 34. The optical spectra are normalised as a group to the peak spectral power at 2.6 MHz

Radio-frequency (RF) spectra of our laser are shown in Figure 37(a) along with the optical spectrum of the laser (Figure 37(b)) and the temporal profile of the pump and laser pulses (Figure 37(c)), for selected frequencies around the cavity frequencies (2.6 MHz). At 2.42 MHz, the laser pulse is approaching the cavity frequency; we can clearly see the second laser line appear at 3.1 µm near to 3.16 µm laser line. In the temporal profile, laser pulses are asynchronies with the pump pulse at

90

2.42 MHz. The lasing pulses lagged behind the pump pulses due to the delay in the arrival of the feedback pulse.

When synchronously pumped (2.6 MHz) the RF spectra reproduce the noise characteristics of the modulated pump source: at other repetition rates they reveal the complex dynamics of asynchronous pumping. When pump and laser pulses in synchronise, the second lasing line a quenching and the main lasing line dominates the laser. In this condition, a laser pulse is more efficient and stable. When the repetition rate increases above the cavity frequency (e.g., 2.7 MHz), a rapid decrease in the output indicates that the decay of the excited state is rapid even at low pulse energies. In C_2H_2 molecules, as there is no radiative transition between the lower laser level vibrational state and the ground state, the faster repetition rates may leave insufficient time for relaxation of the lower level population.

Table 7 summarises our RF and time-dependent measurements of the pump and lasing pulses at different repetition rates. Using the information from Figure 34, the repetition rates which produced extreme output powers (local minimum/maximum) were selected for RF and temporal measurements in Table 7 (except 2.42 MHz). There are slight variations in the repetition rate shown in Table 7 and Figure 34 due to changes in the room temperature and re-cleaving the fibre end face. The overall performance of the pump source at different repetition rates was stable. For synchronous pumping, RF spectra of the lasing pulses were broadly similar to those of the pump, but differences arose due to changing pulse shapes. There were more significant differences away from synchronous pumping and around frequencies corresponding to harmonic, sub-harmonic and fractional harmonic operation.

At 1.4 MHz and 2.7 MHz, which corresponded to the minimum power points in Figure 34, and 1.68 MHz and 3.74 MHz, which were around fractional harmonics of natural cavity frequency, the RF spectra of lasing became noisy and sub-peaks were found between the main peaks. In those conditions, the time-dependent measurements showed that the lasing pulses lagged behind the pump pulses due to the delay in the arrival of the feedback pulse. This was usually accompanied by large pulse timing jitter. At 2.6 MHz and 5.2 MHz, which were near the natural cavity frequency and sub-harmonic frequency, the RF spectra were similar to the pump. Such similarity could also be found at 1.28 MHz, which was near half of the natural frequency. The temporal traces show that the laser and pump pulses were synchronised. The RF and time-dependent measurements supply various information of lasing operation and reveal complex dynamics of the laser system.

All RF and time-dependent measurements used a home-made high-speed HgCdTe detector (*Vigo PVI-3.4-1×1- TO39-No Window-35, 1ns rise time*) for 3.1 µm and a high-speed InGaAs detector (*Thorlabs DET01CFC)* for 1.5 µm. A 350 MHz digital oscilloscope (*Agilent InfiniiVision DSO-X-3032A*) and 6 GHz spectrum analyser (*Agilent CSA Spectrum Analyzer*) were used for measurements. The spectral measurements were used a liquid-nitrogen-cooled InAs detector (*Electro-Optical Systems S-010-LN4*).

Table 7 RF and time dependence measurements.

	1.28 MHz	1.4 MHz
Full Span : 100kHz to 50MHz Resolution: 50kHz		
Full Span : 100kHz to 20MHz Resolution: 20kHz		
Full Span : 100kHz to 10MHz Resolution: 10kHz		
Span : 1kHz Resolution: 10Hz		
	Frequency (MHz)	Frequency (MHz)
Oscilloscope trace		
	Time (ns)	Time (ns)

	1.68 MHz	2.42 MHz
Full Span : 100kHz to 50MHz Resolution: 50kHz		
Full Span : 100kHz to 20MHz Resolution: 20kHz		
Full Span : 100kHz to10MHz Resolution: 10kHz		
Span : 1kHz Resolution: 10Hz	Frequency (MHz)	Frequency (MHz)
Oscilloscope trace	Time (ns)	Time (ns)

	2.6 MHz	2.7 MHz
Full Span : 100kHz to 50MHz Resolution: 50kHz		
Full Span : 100kHz to 20MHz Resolution: 20kHz		
Full Span : 100kHz to 10MHz Resolution: 10kHz		
Span : 1kHz Resolution: 10Hz		
	Frequency (MHz)	Frequency (MHz)
Oscilloscope trace		
	Time (ns)	Time (ns)

	3.74 MHz	5.1 MHz
Full Span : 100kHz to 50MHz Resolution: 50kHz		
Full Span : 100kHz to 20MHz Resolution: 20kHz		
Full Span : 100kHz to 10MHz Resolution: 10kHz		
Span : 1kHz Resolution: 10Hz		
	Frequency (MHz)	Frequency (MHz)
Oscilloscope trace		
	Time (ns)	Time (ns)

6.2.3 Stability of pulsed lasing output

As we mention the important to have stable laser system in the CW operation. Stability of the pulsed laser output (Figure 38) as a function of time also was measured over more than an hour. No frequency locking of the pump or stabilisation or isolation of the laser cavity was used. The pump power was 75 mW on the P (9) transition. The pump repetition rate was 2.6 MHz. The pressure of acetylene gas was 0.25 mbar. 70% output coupler was used and the output power was about 4 mW. A high gain detector (*Thorlab PDA20H-EC*) was used to measure the lasing power directly. Power data was recorded at 10 Hz sampling rate.
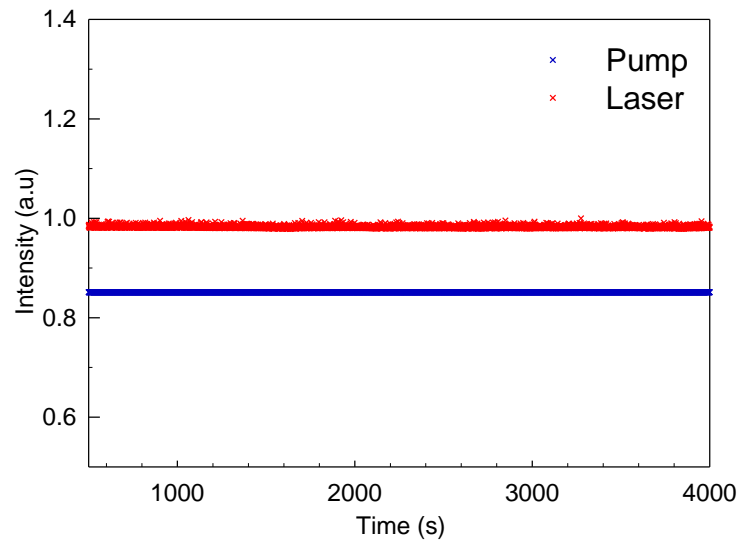
Figure 38 Stability of pulsed output power over time. The pump power was 75 mW on the P9 transition. The repetition rate of the pump was 2.5 MHz. The pressure of acetylene gas was 0.3 mbar. 70% output coupler was used and achieved about 4 mW output power.

6.2.4 Characterisation of laser rings cavity
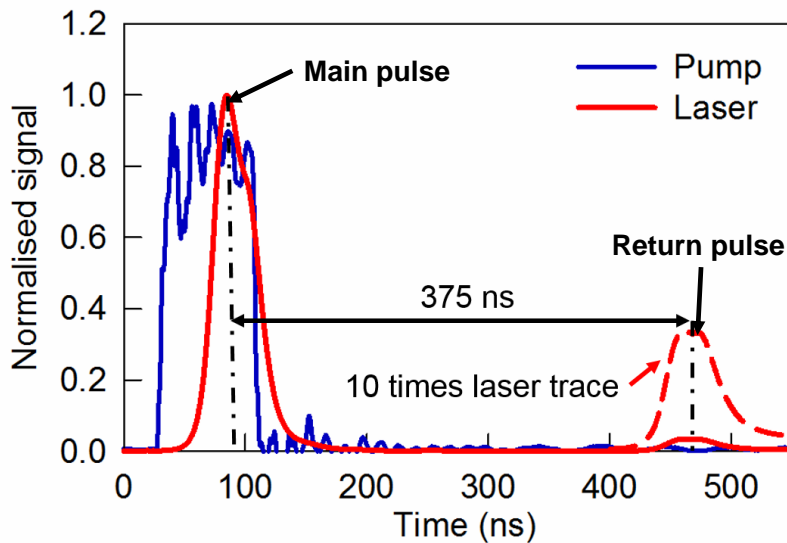
Figure 39 Temporal measurement of laser pulse when pump rate was 1.25 MHz and 70 % output coupler was used. The laser peak after 375nm delay is the circulating pulse in the cavity. The time delay of 375 ns implies a total cavity length of 112 m. The trace shows that the round-trip cavity transmission is 3.4% including 70% output coupling.

The length and loss features of the ring laser cavity can be determined by the temporal measurement of the laser output in the pulsed operation. Figure 39 showed the measured time dependence of laser pulses when pump rate was 1.25 MHz, less than half of the cavity repetition rate (the cavity repetition rate is 2.6 MHz). In Figure 39, a pulse is observed after circulating once in the cavity, 375 ns after the main pulse. The dashed curve shows the return pulse at 10 times higher sensitivity of the oscilloscope. The 375 ns time delay implies that the cavity length was around 112 m including the two fibre lengths and the optical paths through the free-space optics. We can make this estimate because the group index of the fibres used is known to be very close to unity. The amplitude ratio of the pulses is 0.034 which we attribute to the cavity loss of 9.5 dB and 70 % coupling of the output coupler. Time-dependent measurements

98

were performed using an in-house made high-speed HgCdTe detector (*Vigo PVI-3.4-1×1-TO39-NO WINDOW-35, 1 ns rise time*) for 3.1 μm and 6 GHz spectrum analyser (*Agilent CSA Spectrum Analyzer*).

6.3 Summary

In Chapter 6 we described a synchronously pumped mid-IR hollow core fibre gas laser with low threshold running stably around 3 μm wavelength. The cavity repetition rate was recorded is around 2.6 MHz. The laser is enabled by the remarkable properties of mid-IR hollow-core fibre formed from silica and is pumped around 1.53 μm wavelength. We have demonstrated that the system is highly stable over long periods, despite the absence of any external control loop, in synchronously-pumped configurations.

CHAPTER 7

7.1 Conclusions

In this thesis describes the demonstration of a new form of the mid-infrared fibre laser. This molecular gas laser, based on the use of acetylene in high-performance silica hollow core fibre, lases either continuous wave or synchronously pumped when pumped by telecoms-wavelength diode lasers. We have demonstrated the following:

1. A stable continuous wave and pulse lasing in mid-infrared (3.1-3.2 microns) from a molecular gas in a hollow fibre. Our fibre-based laser has a single-mode output beam and an output power of several milliwatts, making it a competitive technology for laser development in the spectral band beyond 3 microns.

2. Low-loss hollow-core fibre at the laser wavelength, (3.16 μm) was fabricated. The attenuation of 0.02 dB/m was recorded. This fibre has one of the lowest attenuations reported for any optical fibre in this spectral band, enabling long optical cavities and, hence, low-repetition-rate pulsed lasing.

3. A laser system that we develop was based on pumping using telecoms diode lasers. In one configuration, our laser has a remarkably low threshold of below 20mW and so can easily lase when pumped by an unamplified diode laser with standard telecoms grade stabilisation.

4. We have demonstrated that the system is highly stable over long periods, despite the absence of any external control loop, in both CW and synchronously-pumped configurations.

7.2 Future Work

The development of fibre lasers emitting in the mid-infrared is a growing field of photonics that has already demonstrated in this report, but still many efforts of additional investigations to extend the work presented in this report. Among them are:

1. We have demonstrated lasing on some transitions in the spectral band 3.1 – 3.2 µm using acetylene molecules. The system could also be extended to different wavelengths using other molecular gain systems up to 5 µm wavelength.

2. On the other hand, telecoms-band technology makes it straightforward to amplify the pump and output to far higher powers and to modulate the pump over a broad frequency range. In the next steps for our research, we will demonstrate the use of this technology as an optical amplifier, and then use a much higher-power pump laser to increase the output power. Recently, we demonstrate 0.47 W of continuous wave 3.1 µm output from an acetylene-filled hollow-core fibre when pumped by a high power pump diode-seeded EDFA. This result has been submitted to the international conference.

3. Although we success on demonstrating the continuous wave (CW) laser in 3-micron region using this system, but the physics of the continuous wave (CW) lasing of mid-IR hollow core fibre gas laser based on population inversion stayed elusive. This remains one of the most interesting and promising areas to continue investigating.

REFERENCES

[1] R. Gould, "The LASER, light amplification by stimulated emission of radiation." The Ann Arbor conference on optical pumping, the University of Michigan. Vol. 15. 1959.

[2] T. H. Maiman, "Stimulated Optical Radiation in Ruby," *Nature*, vol. 187, no. 4736, pp. 493–494, Aug. 1960.

[3] A. Einstein, "Concerning an heuristic point of view toward the emission and transformation of light," *Ann. Phys.*, vol. 17, pp. 132–148, 1905.

[4] J. Baxter, "Semiconductor lasers: Pushing the mid-infrared," *Nat. Photonics*, vol. 6, no. 4, pp. 212–212, Mar. 2012.

[5] Daylight Solutions » Daylight Solutions' Products Based On ECqcL(TM) Technology." [Online]. Available: http://www.daylightsolutions.com/products/. [Accessed: 18-Apr-2016].

[6] R. Colombelli, K. Srinivasan, M. Troccoli, O. Painter, C. F. Gmachl, D. M. Tennant, A. M. Sergent, D. L. Sivco, A. Y. Cho, and F. Capasso, "Quantum cascade surface-emitting photonic crystal laser.," *Science*, vol. 302, no. 5649, pp. 1374–7, Nov. 2003.

[7] I. Vurgaftman and J. R. Meyer, "Analysis of limitations to wallplug efficiency and output power for quantum cascade lasers," *J. Appl. Phys.*, vol. 99, no. 12, p. 123108, Jun. 2006.

[8] M. I. Buchwald, C. R. Jones, H. R. Fetterman, and H. R. Schlossberg, "Direct optically pumped multiwavelength CO_2 laser," *Appl. Phys. Lett.*, vol. 29, no. 5, p. 300, Aug. 1976.

[9] T. Y. Chang and O. R. Wood, "Optically pumped 33-atm CO_2 laser," *Appl. Phys. Lett.*, vol. 23, no. 7, p. 370, 1973.

[10] Z. Wang, W. Belardi, F. Yu, W. J. Wadsworth, and J. C. Knight, "Efficient diode-pumped mid-infrared emission from acetylene-filled hollow-core fiber," *Opt. Express*, vol. 22, no. 18, p. 21872, 2014.

[11] J. E. McCord, H. C. Miller, G. Hager, A. I. Lampson, and P. G. Crowell, "Experimental investigation of an optically pumped mid-infrared carbon monoxide laser," *IEEE J. Quantum Electron.*, vol. 35, no. 11, pp. 1602–1612, 1999.

[12] C. Jauregui, J. Limpert, and A. Tünnermann, "High-power fibre lasers," *Nat. Photonics*, vol. 7, no. 11, pp. 861–867, Oct. 2013.

[13] H. M. Pask, R. J. Carman, D. C. Hanna, A. C. Tropper, C. J. Mackechnie, P. R. Barber, and J. M. Dawes, "Ytterbium-doped silica fiber lasers: versatile sources for the 1-1.2 μm region," *IEEE J. Sel. Top. Quantum Electron.*, vol. 1, no. 1, pp. 2–13, Apr. 1995.

[14] S. D. Jackson, "Towards high-power mid-infrared emission from a fibre laser," *Nat. Photonics*, vol. 6, no. 7, pp. 423–431, Jun. 2012.

[15] J. Li, D. D. Hudson, and S. D. Jackson, "High-power diode-pumped fiber laser operating at 3 μm.," *Opt. Lett.*, vol. 36, no. 18, pp. 3642–4, Sep. 2011.

[16] F. Yu, W. J. Wadsworth, and J. C. Knight, "Low loss silica hollow core fibers for 3-4 μm spectral region.," *Opt. Express*, vol. 20, no. 10, pp. 11153–8, May 2012.

[17] P. Smith, "Stabilized, single-frequency output from a long laser cavity," *IEEE J. Quantum Electron.*, vol. 1, no. 8, pp. 343–348, Nov. 1965.

[18] T. Y. Chang and T. J. Bridges, "Laser action at 452, 496, and 541 μm in optically pumped CH3F," *Opt. Commun.*, vol. 1, no. 9, pp. 423–426, Apr. 1970.

[19] T. Y. Chang and O. R. Wood, "Optically pumped atmospheric-pressure CO2 laser," *Appl. Phys. Lett.*, vol. 21, no. 1973, pp. 19–21, 1972.

[20] H. R. Schlossberg and H. R. Fetterman, "Optically pumped vibrational transition laser in OCS," *Appl. Phys. Lett.*, vol. 26, no. 6, p. 316, Sep. 1975.

[21] T. Ehrenreich, "Diode Pumped Cesium Laser," *Am. Phys. Soc.*, 2005.

[22] J. E. McCord, H. C. Miller, G. Hager, A. I. Lampson, and P. G. Crowell, "Experimental investigation of an optically pumped mid-infrared carbon monoxide laser," *IEEE J. Quantum Electron.*, vol. 35, no. 11, pp. 1602–1612, 1999.

[23] J. E. McCord, A. A. Ionin, S. P. Phipps, P. G. Crowell, A. I. Lampson, J. K. McIver, A. J. W. Brown, and G. D. Hager, "Frequency-tunable optically pumped carbon monoxide laser," *IEEE J. Quantum Electron.*, vol. 36, no. 9, pp. 1041–1052, Sep. 2000.

[24] H. C. Miller, D. T. Radzykewycz, and G. Hager, "An optically pumped mid-infrared HBr laser," *IEEE J. Quantum Electron.*, vol. 30, no. 10, pp. 2395–2400, 1994.

[25]   A. V. V. Nampoothiri, a Ratanavis, N. Campbell, and W. Rudolph, "Molecular C_2H_2 and HCN lasers pumped by an optical parametric oscillator in the 1 . 5-μm band," *Opt. Express*, vol. 18, no. 3, pp. 1946–1951, 2010.

[26]   J. Zweiback, A. Komashko, and W. F. Krupke, "Alkali-vapor lasers," in *SPIE LASE*, 2010, p. 75810G–75810G–5.

[27]   W. F. Krupke, R. J. Beach, V. K. Kanz, and S. A. Payne, "Resonance transition 795-nm rubidium laser," *Opt. Lett.*, vol. 28, no. 23, p. 2336, Dec. 2003.

[28]   B. V. Zhdanov, T. Ehrenreich, and R. J. Knize, "Highly efficient optically pumped cesium vapor laser," *Opt. Commun.*, vol. 260, no. 2, pp. 696–698, Apr. 2006.

[29]   D. J.F., *Rare-Earth-Doped Fiber Lasers and Amplifiers, Revised and Expanded*. CRC Press, 1993, p. 798.

[30]   A. Javan, W. R. Bennett, and D. R. Herriott, "Population inversion and continuous optical maser oscillation in a gas discharge containing a He-Ne mixture," *Phys. Rev. Lett.*, vol. 6, pp. 106–110, 1961.

[31]   A. V. V. Nampoothiri, B. Debord, M. Alharbi, F. Gérôme, F. Benabid, and W. Rudolph, "CW hollow-core optically pumped I 2 fiber gas laser," *Opt. Lett.*, vol. 40, no. 4, pp. 605–608, 2015.

[32]   A. M. Jones, A. V. V. Nampoothiri, A. Ratanavis, T. Fiedler, N. V. Wheeler, F. Couny, R. Kadel, F. Benabid, B. R. Washburn, K. L. Corwin, and W. Rudolph, "Mid-infrared gas filled photonic crystal fiber laser based on population inversion," *Opt. Express*, vol. 19, no. 3, p. 2309, Jan. 2011.

[33]   W. C. Swann and S. L. Gilbert, "Pressure-induced shift and broadening of 1510–1540-nm acetylene wavelength calibration lines," *J. Opt. Soc. Am. B*, vol. 17, no. 7, p. 1263, Jul. 2000.

[34]   A. M. Smith, S. L. Coy, W. Klemperer, and K. K. Lehmann, "Fourier transform spectra of overtone bands of HCN from 5400 to 15100 cm−1," *J. Mol. Spectrosc.*, vol. 134, no. 1, pp. 134–153, Mar. 1989.

[35]   A. V. V. Nampoothiri, A. M. Jones, C. Fourcade-Dutin, C. Mao, N. Dadashzadeh, B. Baumgart, Y. Y. Wang, M. Alharbi, T. Bradley, N. Campbell, F. Benabid, B. R. Washburn, K. L. Corwin, and W. Rudolph, "Hollow-core Optical Fiber Gas Lasers (HOFGLAS): a review [Invited]," *Opt. Mater. Express*, vol. 2, no. 7, p. 948, Jun. 2012.

[36]   J. A. Stregack, B. L. Wexler, and G. A. Hart, "CW CO-CS_2, CO-C_2H_2, and CO-N_2O energy-transfer lasers," *Appl. Phys. Lett.*, vol. 28, no. 3, p. 137, Aug. 1976.

[37] H. Kildal and T. F. Deutsch, "Optically pumped infrared V-V transfer lasers," *Appl. Phys. Lett.*, vol. 27, no. 9, p. 500, Sep. 1975.

[38] A. M. Jones, a V. V. Nampoothiri, A. Ratanavis, R. Kadel, N. V Wheeler, F. Couny, F. Benabid, W. Rudolph, B. R. Washburn, and K. L. Corwin, "C_2H_2 Gas Laser Inside Hollow-Core Photonic Crystal Fiber Based on Population Inversion," In *Conference on Lasers and Electro-Optics* (p. CTuU1). Optical Society of America,2010.

[39] A. M. Jones, A. V. V. Nampoothiri, T. Fiedler, R. Kadel, W. Hageman, N. Wheeler, F. Couny, F. Benabid, W. Rudolph, K. L. Corwin, and B. R. Washburn, "Mid-IR fiber lasers based on molecular gas-filled hollow-core photonic crystal fiber," *In CLEO: Science and Innovations*, (p. CThD1). Optical Society of America, 2011.

[40] M. C. Heaven, J. Han, and K. Freel, "Rotational and Vibrational Energy Transfer from the First Overtone Strech of Acetylene," *"International Symp. Mol. Spectrosc.*, 2010.

[41] W. C. Swann and S. L. Gilbert, "Pressure-induced shift and broadening of 1510–1540-nm acetylene wavelength calibration lines," *J. Opt. Soc. Am. B*, vol. 17, no. 7, p. 1263, Jul. 2000.

[42] R. Amarin, "Theoretical and experimental studies of optically pumped molecular gas lasers." 01-May-2010.

[43] I. W. M. Smith and J. F. Warr, "Vibrational relaxation of C2H2(v_3,v_2+v_4+v_5) in self-collisions and in collisions with the noble gases," *Chem. Phys. Lett.*, vol. 173, no. 1, pp. 70–75, Sep. 1990.

[44] J. R. Carson, S. P. Mead, and S. A. Schelkunoff, "Hyper-Frequency Wave Guides-Mathematical Theory," *Bell Syst. Tech. J.*, vol. 15, no. 2, pp. 310–333, Apr. 1936.

[45] E. A. J. Marcatili and R. A. Schmeltzer, "Hollow Metallic and Dielectric Waveguides for Long Distance Optical Transmission and Lasers," *Bell Syst. Tech. J.*, vol. 43, no. 4, pp. 1783–1809, Jul. 1964.

[46] J. C. Knight, J. Broeng, T. A. Birks, and P. S. J. Russell, "Photonic Band Gap Guidance in Optical Fibers," *Science (80-.).*, vol. 282, no. 5393, 1998.

[47] P. S. J. Russell, "Photonic-Crystal Fibers," *J. Light. Technol.*, vol. 24, no. 12, pp. 4729–4749, Dec. 2006.

[48] P. J. Roberts, F. Couny, H. Sabert, B. J. Mangan, D. P. Williams, L. Farr, M. W. Mason, A. Tomlinson, T. A. Birks, J. C. Knight, and P. St. J. Russell, "Ultimate low loss of hollow-core photonic crystal fibres," *Opt. Express*, vol. 13, no. 1, p. 236, 2005.

[49] P. Jaworski, F. Yu, R. R. J. Maier, W. J. Wadsworth, J. C. Knight, J. D. Shephard, and D. P. Hand, "Picosecond and nanosecond pulse delivery through a hollow-core Negative Curvature Fiber for micro-machining applications.," *Opt. Express*, vol. 21, no. 19, pp. 22742–53, 2013.

[50] D. G. Ouzounov, F. R. Ahmad, D. Müller, N. Venkataraman, M. T. Gallagher, M. G. Thomas, J. Silcox, K. W. Koch, and A. L. Gaeta, "Generation of megawatt optical solitons in hollow-core photonic band-gap fibers.," *Science*, vol. 301, no. 5640, pp. 1702–4, Sep. 2003.

[51] F. Benabid, J. C. Knight, G. Antonopoulos, and P. S. J. Russell, "Stimulated Raman Scattering in Hydrogen-Filled Hollow-Core Photonic Crystal Fiber," *Science (80).*, vol. 298, no. 5592, 2002.

[52] F. Benabid and P. J. Roberts, "Linear and nonlinear optical properties of hollow core photonic crystal fiber," *J. Mod. Opt.*, vol. 58, no. 2, pp. 87–124, Jan. 2011.

[53] N. V. Wheeler, A. M. Heidt, N. K. Baddela, E. N. Fokoua, J. R. Hayes, S. R. Sandoghchi, F. Poletti, M. N. Petrovich, and D. J. Richardson, "Low-loss and low-bend-sensitivity mid-infrared guidance in a hollow-core-photonic-bandgap fiber.," *Opt. Lett.*, vol. 39, no. 2, pp. 295–8, 2014.

[54] F. Yu and J. C. Knight, "Spectral attenuation limits of silica hollow core negative curvature fiber.," *Opt. Express*, vol. 21, no. 18, pp. 21466–71, 2013.

[55] J. Bei, T. M. Monro, A. Hemming, and H. Ebendorff-Heidepriem, "Reduction of scattering loss in fluoroindate glass fibers," *Opt. Mater. Express*, vol. 3, no. 9, p. 1285, 2013.

[56] W. H. Kim, V. Q. Nguyen, L. B. Shaw, L. E. Busse, C. Florea, D. J. Gibson, R. R. Gattass, S. S. Bayya, F. H. Kung, G. D. Chin, R. E. Miklos, I. D. Aggarwal, and J. S. Sanghera, "Recent progress in chalcogenide fiber technology at NRL," *J. Non. Cryst. Solids*, vol. 431, pp. 8–15, 2016.

[57] F. Yu, J. Knight, "Negative curvature hollow core optical fiber," *IEEE J. Sel. Top. Quantum Electron.* IEEE 22, no. 2 (2016): 1-11.

[58] J. D. Shephard, A. Urich, R. M. Carter, P. Jaworski, R. R. J. Maier, W. Belardi, F. Yu, W. J. Wadsworth, J. C. Knight, and D. P. Hand, "Silica hollow core microstructured fibers for beam delivery in industrial and medical applications," *Front. Phys.*, vol. 3, Apr. 2015.

[59] C. Harvey, F. Yu, J. C. Knight, W. Wadsworth, and P. Almeida, "Reducing Nonlinear Limitations of Ytterbium Mode-Locked Fibre Lasers with Hollow-Core Negative Curvature Fibre," in *CLEO: 2015*, p. STh1L.5.

[60]   Z. Wang, F. Yu, W. J. Wadsworth, and J. C. Knight, "Efficient 1.9 μ m emission in H 2 -filled hollow core fiber by pure stimulated vibrational Raman scattering," *Laser Phys. Lett.*, vol. 11, no. 10, p. 105807, Oct. 2014.

[61]   V. Setti, L. Vincetti, and A. Argyros, "Flexible tube lattice fibers for terahertz applications.," *Opt. Express*, vol. 21, no. 3, pp. 3388–99, Feb. 2013.

[62]   A. N. Kolyadin, A. F. Kosolapov, A. D. Pryamikov, A. S. Biriukov, V. G. Plotnichenko, and E. M. Dianov, "Light transmission in negative curvature hollow core fiber in extremely high material loss region.," *Opt. Express*, vol. 21, no. 8, pp. 9514–9, Apr. 2013.

[63]   W. Belardi and J. C. Knight, "Hollow antiresonant fibers with reduced attenuation.," *Opt. Lett.*, vol. 39, no. 7, pp. 1853–6, Apr. 2014.

[64]   V. S. Shiryaev, "Chalcogenide Glass Hollow-Core Microstructured Optical Fibers," *Front. Mater.*, vol. 2, Mar. 2015.

[65]   Y. Y. Wang, F. Couny, P. J. Roberts, and F. Benabid, "Low loss broadband transmission in optimized core-shape Kagome hollow-core PCF," *Lasers Electro-Optics Quantum Electron. Laser Sci. Conf. (QELS), 2010 Conf.*, pp. 4–5, 2010.

[66]   Y. Y. Wang, N. V Wheeler, F. Couny, P. J. Roberts, and F. Benabid, "Low loss broadband transmission in hypocycloid-core Kagome hollow-core photonic crystal fiber.," *Opt. Lett.*, vol. 36, no. 5, pp. 669–671, 2011.

[67]   A. D. Pryamikov, A. S. Biriukov, A. F. Kosolapov, V. G. Plotnichenko, S. L. Semjonov, and E. M. Dianov, "Demonstration of a waveguide regime for a silica hollow--core microstructured optical fiber with a negative curvature of the core boundary in the spectral region > 3.5 μm.," *Opt. Express*, vol. 19, no. 2, pp. 1441–8, Jan. 2011.

[68]   W. Belardi and J. C. Knight, "Hollow antiresonant fibers with low bending loss.," *Opt. Express*, vol. 22, no. 8, pp. 10091–6, Apr. 2014.

[69]   V. Setti, L. Vincetti, and a Argyros, "Flexible tube lattice fibers for terahertz applications.," *Opt. Express*, vol. 21, no. 3, pp. 3388–99, Feb. 2013.

[70]   A. Urich, R. R. J. Maier, F. Yu, J. C. Knight, D. P. Hand, and J. D. Shephard, "Flexible delivery of Er:YAG radiation at 2.94 μm with negative curvature silica glass fibers: a new solution for minimally invasive surgical procedures.," *Biomed. Opt. Express*, vol. 4, no. 2, pp. 193–205, Feb. 2013.

[71] A. Urich, R. R. J. Maier, F. Yu, J. C. Knight, D. P. Hand, and J. D. Shephard, "Silica hollow core microstructured fibres for mid-infrared surgical applications," *J. Non. Cryst. Solids*, vol. 377, pp. 236–239, Oct. 2013.

[72] B. Debord, M. Alharbi, T. Bradley, C. Fourcade-Dutin, Y. Y. Wang, L. Vincetti, F. Gérôme, and F. Benabid, "Hypocycloid-shaped hollow-core photonic crystal fiber Part I: arc curvature effect on confinement loss.," *Opt. Express*, vol. 21, no. 23, pp. 28597–608, Nov. 2013.

[73] M. Alharbi, T. Bradley, B. Debord, C. Fourcade-Dutin, D. Ghosh, L. Vincetti, F. Gérôme, and F. Benabid, "Hypocycloid-shaped hollow-core photonic crystal fiber Part II: cladding effect on confinement and bend loss.," *Opt. Express*, vol. 21, no. 23, pp. 28609–16, Nov. 2013.

[74] M. A. Duguay, Y. Kokubun, T. L. Koch, and L. Pfeiffer, "Antiresonant reflecting optical waveguides in SiO2-Si multilayer structures," *Appl. Phys. Lett.*, vol. 49, no. 1, p. 13, Jul. 1986.

[75] T. P. White, R. C. McPhedran, C. Martijnde Sterke, N. M. Litchinitser, and B. J. Eggleton, "Resonance and scattering in microstructured optical fibers.," *Opt. Lett.*, vol. 27, no. 22, pp. 1977–9, Nov. 2002.

[76] N. M. Litchinitser, S. C. Dunn, B. Usner, B. J. Eggleton, T. P. White, R. C. McPhedran, and C. M. de Sterke, "Resonances in microstructured optical waveguides.," *Opt. Express*, vol. 11, no. 10, pp. 1243–51, May 2003.

[77] N. M. Litchinitser, A. K. Abeeluck, C. Headley, and B. J. Eggleton, "Antiresonant reflecting photonic crystal optical waveguides," *Opt. Lett.*, vol. 27, no. 18, p. 1592, Sep. 2002.

[78] A. W. Snyder and J. Love, *Optical Waveguide Theory*. Springer Science & Business Media, 2012, p. 738.

[79] F. Couny, F. Benabid, P. J. Roberts, M. T. Burnett, and S. A. Maier, "Identification of Bloch-modes in hollow-core photonic crystal fiber cladding," *Opt. Express*, vol. 15, no. 2, p. 325, Jan. 2007.

[80] L. Vincetti and V. Setti, "Waveguiding mechanism in tube lattice fibers.," *Opt. Express*, vol. 18, no. 22, pp. 23133–46, Oct. 2010.

[81] T. A. Birks, G. J. Pearce, and D. M. Bird, "Approximate band structure calculation for photonic bandgap fibres.," *Opt. Express*, vol. 14, no. 20, pp. 9483–90, Oct. 2006.

[82] A. Argyros and J. Pla, "Hollow-core polymer fibres with a kagome lattice: potential for transmission in the infrared," *Opt. Express*, vol. 15, no. 12, p. 7713, 2007.

[83] L. Vincetti and V. Setti, "Extra loss due to Fano resonances in inhibited coupling fibers based on a lattice of tubes," *Opt. Express*, vol. 20, no. 13, p. 14350, Jun. 2012.

[84] W. Belardi and J. C. Knight, "Effect of core boundary curvature on the confinement losses of hollow antiresonant fibers," *Opt. Express*, vol. 21, no. 19, p. 21912, Sep. 2013.

[85] F. Yu and J. C. Knight, "Spectral attenuation limits of silica hollow core negative curvature fiber.," *Opt. Express*, vol. 21, no. 18, pp. 21466–71, Sep. 2013.

[86] A. D. Pryamikov, "Negative curvature hollow core fibers: design, fabrication, and applications," In *SPIE LASE*, pp. 89610I-89610I. International Society for Optics and Photonics, 2014

[87] T. J. Birks, T. A., Roberts, P. J., Russell, P. S. J., Atkin, D. M. & Shepherd, K. Ishihara, K. Tsujikawa, M. Ohashi, K. Shiraki, and M. Tateda, "Full 2-D photonic bandgaps in silica/air structures," *Electron. Lett.*, vol. 31, no. 22, pp. 1941–1943, 1995.

[88] K. M. Kiang, K. Frampton, T. M. Monro, R. Moore, J. Tucknott, D. W. Hewak, D. J. Richardson, and H. N. Rutt, "Extruded singlemode non-silica glass holey optical fibres," *Electron. Lett.*, vol. 38, no. 12, p. 546, 2002.

[89] V. V. R. Kumar, A. George, W. Reeves, J. Knight, P. Russell, F. Omenetto, and a Taylor, "Extruded soft glass photonic crystal fiber for ultrabroad supercontinuum generation.," *Opt. Express*, vol. 10, no. 25, pp. 1520–5, Dec. 2002.

[90] A. Wang, V. V. R. K. Kumar, A. K. George, J. C. Knight, and P. S. J. Russell, "Extruded tellurite photonic crystal fibre," *Opt. Express, vol* 11, no. 20 (2003): 2641-2645

[91] R. T. Bise and D. J. Trevor, "Sol-gel derived microstructured fiber: fabrication and characterization," *OFC/NFOEC Tech. Dig. Opt. Fiber Commun. Conf. 2005.*, p. 3 pp. Vol. 3, 2005.

[92] M. Van Eijkelenborg, M. Large, a Argyros, J. Zagari, S. Manos, N. Issa, I. Bassett, S. Fleming, R. McPhedran, C. M. de Sterke, and N. A. Nicorovici, "Microstructured polymer optical fibre.," *Opt. Express*, vol. 9, no. 7, pp. 319–27, Sep. 2001.

[93] O. Humbach, H. Fabian, U. Grzesik, U. Haken, and W. Heitmann, "Analysis of OH absorption bands in synthetic silica," *J. Non. Cryst. Solids*, vol. 203, pp. 19–26, Aug. 1996.

[94] Y. Chen and T. A. Birks, "Predicting hole sizes after fibre drawing without knowing the viscosity," *Opt. Mater. Express*, vol. 3, no. 3, p. 346, Feb. 2013.

[95]   U. Haken, O. Humbach, S. Ortner, and H. Fabian, "Refractive index of silica glass: influence of fictive temperature," *J. Non. Cryst. Solids*, vol. 265, no. 1–2, pp. 9–18, Mar. 2000.

[96]   M. R. Abu Hassan, F. Yu, W. J. Wadsworth, and J. C. Knight, "Cavity-based mid-IR fiber gas laser pumped by a diode laser," *Optica*, vol. 3, no. 3, p. 218, Mar. 2016.

[97]   T. Y. Chang, "Optically pumped 33-atm CO2 laser," *Appl. Phys. Lett.*, vol. 23, no. 7, p. 370, Oct. 1973.

[98]   R. F. Cregan, "Single-Mode Photonic Band Gap Guidance of Light in Air," *Science (80-.).*, vol. 285, no. 5433, pp. 1537–1539, Sep. 1999.

[99]   A. M. Jones, a V. V. Nampoothiri, A. Ratanavis, T. Fiedler, N. V Wheeler, F. Couny, R. Kadel, F. Benabid, B. R. Washburn, K. L. Corwin, and W. Rudolph, "Mid-infrared gas filled photonic crystal fiber laser based on population inversion.," *Opt. Express*, vol. 19, no. 3, pp. 2309–2316, 2011.

[100] M. C. Heaven, J. Han, and K. Freel, "Rotational And Vibrational Energy Transfer From The First Overtone Strech Of Acetylene." Ohio State University, 2010.

[101] A. Ratanavis, N. Campbell, and W. Rudolph, "Feasibility study of optically pumped molecular lasers with small quantum defect," *Opt. Commun.*, vol. 283, no. 6, pp. 1075–1080, Mar. 2010.

[102] "HITRAN." [Online]. Available: cfa-www.harvard.edu/hitran/.

[103] A. E. Siegman, "<title>Defining, measuring, and optimizing laser beam quality</title>," in *OE/LASE'93: Optics, Electro-Optics, & Laser Applications in Science& Engineering*, 1993, pp. 2–12.

[104] U. Keller and R. Hibst, "Experimental studies of the application of the Er:YAG laser on dental hard substances: II. Light microscopic and SEM investigations," *Lasers Surg. Med.*, vol. 9, no. 4, pp. 345–351, 1989.

[105] J. D. Shephard, P. J. Roberts, J. D. C. Jones, J. C. Knight, and D. P. Hand, "Measuring Beam Quality of Hollow Core Photonic Crystal Fibers," *J. Light. Technol. Vol. 24, Issue 10, pp. 3761-3769*, vol. 24, no. 10, pp. 3761–3769, 2006.

[106] V. Nampoothiria, A. M. Jones, A. Ratanavis, N. Campbella, R. Kadel, N. Wheeler, F. Couny, F. Benabid, B. R. Washburn, K. L. Corwin, and W. Rudolph, "Optically pumped C2H2 and HCN lasers with conventional cavities and based on hollow core photonic crystal fibers," *AIP Conf. Proc.*, vol. 1278, no. 2010, pp. 749–757, 2010.

List of publications

Journal:

1. Muhammad Rosdi Abu Hassan, Fei Yu, William J. Wadsworth, and Jonathan C. Knight, "Cavity-based mid-IR fiber gas laser pumped by a diode laser," Optica 3, 218-221 (2016)

Conferences & Proceedings:

1. F. Yu, M. R. A. Hassan, W. J. Wadsworth, and J. C. Knight, "Line-tunable CW Lasing of Mid-infrared Acetylene Gas Hollow Core Fiber Laser," in *Conference on Lasers and Electro-Optics*, OSA Technical Digest (2016) (Optical Society of America, 2016), paper STh1O.2.

2. J. C. Knight, R. Hassan, F. Yu, and W. J. Wadsworth, "Hollow core fibers for optically pumped mid-IR fiber lasers," in *Workshop on Specialty Optical Fibers and Their Applications*, OSA Technical Digest (online) (Optical Society of America, 2015), paper WF2A.1.

3. M. R. Abu Hassan, F. Yu, Z. Wang, W. Belardi, W. Wadsworth, and J. Knight, "Synchronously Pumped Mid-IR Hollow Core Fiber Gas Laser," in *CLEO: 2015*, OSA Technical Digest (online) (Optical Society of America, 2015), paper SF1F.7.

4. Wadsworth, W., Love, A., Bateman, S., Yu, F., Abu Hassan, M. R. and Knight, J., 2015. Lasers Using Low Loss Hollow Optical Fibres in the Mid-Infrared. In: OECC, (2015).

5. M. R. Abu Hassan and J. C. Knight, "Controlling the Transmission Bandwidth in All-Solid PBG Fibre through Cladding Design," in *Workshop on Specialty Optical Fibers and their Applications*, (Optical Society of America, 2013), (poster).